2005

X-ray absorption spectral study of metal to insulator transition in $NiS_{1.38}Se_{0.62}$

Quang Van Le
San Jose State University

Follow this and additional works at: https://scholarworks.sjsu.edu/etd_theses

Recommended Citation

Le, Quang Van, "X-ray absorption spectral study of metal to insulator transition in $NiS_{1.38}Se_{0.62}$" (2005). *Master's Theses*. 2771.
DOI: https://doi.org/10.31979/etd.ynkw-pxd4
https://scholarworks.sjsu.edu/etd_theses/2771

NOTE TO USERS

UMI®

X-RAY ABSORPTION SPECTRAL STUDY OF METAL TO

INSULATOR TRANSITION IN $NiS_{1.38}Se_{0.62}$

A Thesis

Presented to

The Faculty of the Department of Chemistry

San José State University

In partial Fulfillment for the Degree

Master of Science

By

Quang Van Le

August 2005

UMI Number: 1429434

INFORMATION TO USERS

The quality of this reproduction is dependent upon the quality of the copy submitted. Broken or indistinct print, colored or poor quality illustrations and photographs, print bleed-through, substandard margins, and improper alignment can adversely affect reproduction.

In the unlikely event that the author did not send a complete manuscript and there are missing pages, these will be noted. Also, if unauthorized copyright material had to be removed, a note will indicate the deletion.

UMI®
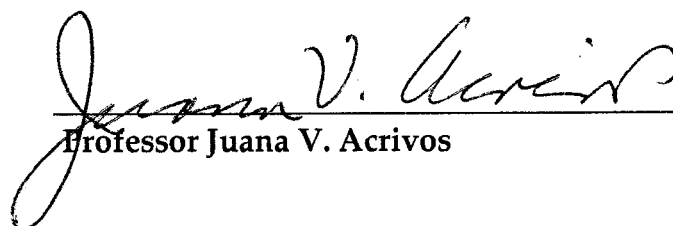
APPROVED FOR THE DEPARTMENT OF CHEMISTRY

Professor Juana V. Acrivos

Professor Carolus Boekema

Professor Roger Terrill

APPROVED FOR THE UNIVERSITY

08/05/05

ABSTRACT

X-RAY ABSORPTION SPECTRAL STUDY OF METAL TO INSULATOR TRANSITION IN $NiS_{1.38}Se_{0.62}$

by Quang Van Le

An anti-ferromagnetic metal (AFM) to weak ferromagnetic insulator (WFI) transition by transmission x-ray absorption spectra (XAS) was investigated for amorphous powder $NiS_{2-x}Se_x$ (x=0.62) at the Se and Ni K Edges in the 2K to 70K temperature range to determine the presence of a temperature dependence for AFM to WFI transition. X-ray temperature difference absorption spectra (XTDAS) relative to 5K for $NiS_{2-x}Se_x$ (x=0.62) over the measured temperature range correlated well with the changes in Extended X-ray Absorption Fine Structure (EXAFS) analysis and the material phase transition diagram obtained from conductivity and magnetic susceptibility data, which exists for $NiS_{2-x}Se_x$ (x=0.62) in the 0.5K to 100K temperature range.

ACKNOWLEDGEMENTS

TABLE OF CONTENTS

LIST OF TABLES

LIST OF FIGURES

1. INTRODUCTION

1.1 Metallic versus Insulator in NiSeS Alloy

The Band-theory (BT) model for free electrons introduced by Wilson[1-2] in 1931 successfully classified materials into metals, semiconductors, and insulators. As shown in Figure 1, where an insulator or semiconductor is a material with an energy gap between the full valence band and the empty conduction band, and metal is a material with a partially occupied valence band or an overlapping conduction and valence bands. Straightforward application of the BT model to nickel disulfide (NiS_2) and nickel diselenide ($NiSe_2$) where the 3d-levels are partially filled would predict metallic properties for both. Albeit, $NiSe_2$ exhibits expected metallic properties, NiS_2, surprisingly shows insulating behavior despite the not completely filled outermost electron shells. Hence, the unexpected insulating property observed in NiS_2 cannot adequately be explained by band theory.

A major weakness of the BT model, which would incorrectly predict metallic properties for NiS_2, assumes that all the valence electrons in a solid are free. The possibility of electrons interacting with atoms of the lattice and/or with other electrons is neglected. In materials where electron interactions exist, the strength of electron-electron interaction (e-e) can explain the insulating property of certain materials such as NiS_2.

A conceptual framework for understanding the role of e-e in solids was first introduced by Mott[3]-Hubbard[4] through an electron correlation model to describe the effect of strong e-e on the material properties of solids. They argued that the insulating behavior of many transition metal compounds such as NiS_2 is due to a large on-site dominant effect of strong electron-electron interaction, which can cause a correlation gap to open in the conduction band. Therefore,

application of Mott-Hubbard's theory to NiS_2 and $NiSe_2$ is ideal to provide insights into the electronic properties of these materials.

The important electron bands for defining material properties are the electrons located in the outermost shells referred to as valence electrons. In the isostructural pyrite series such as $NiSe_2$ and NiS_2, the nickel atom contains eight valence electrons in 3d states. A 3d band would have room for ten electrons. The cubic field can split the 3d states into a doubly degenerate (e_g) level with four states and a triply degenerate (t_{2g}) band with six in a cubic symmetry as shown in Figure 2. The physical properties of these systems evolve with the progressive filling of the nickel 3d bands with electrons and the strength of e-e. As is shown in Figure 3a, with eight electrons filling according to Hund's ground state rule and the Pauli Exclusion Principle, the partial filled e_g band in the 3d state would lead to a partially filled band so metallic behavior is expected. The phenomenon observed in $NiSe_2$ is valid according to Mott[3]-Hubbard[4] model when e-e is not considered. When electron-electron interaction exists, the strong short-range Coulomb repulsion of electrons would split the e_g band resulting in electron energies that lie in a full band and empty one as shown in Figure 2c and Figure 3b. As result, the material would exhibit insulating properties as observed in NiS_2.

Sawatzhy et al[5] later expanded on Mott-Hubbard's work and came up with a description of electron-electron interactions. This model can explain the material properties of NiS_2 and $NiSe_2$. Basically, there are two types of e-e. The first type is electron correlation (U), which is the energy cost for transferring a 3d electron between one Ni^{2+} to another ($3d^n \rightarrow d^{n+1} \rightarrow d^{n-1}$) as shown in Figure 4a. U is described as:

$$U = \left(E_I\left(d^{n-1}\right) - E_A\left(d^n\right) + E_I\left(d^{n+1}\right) - E_A\left(d^n\right)\right) \qquad (1)$$

where d is the 3d state electron and U is related to the difference between the ionization energy (E_I) and the electron affinity (E_A) of the Ni^{2+} ion. Depending on the strength of U, the electron-electron interaction due to cation to cation interaction will have two consequences on the properties of NiS_2. The first consequence is that NiS_2 is an insulator due to the energy gap in the 3d band resulting from strong electron correlation. The second consequence is that bonding in NiS_2 is more ionic in nature due to electron-electron repulsion localizing the 3d electrons to Ni ion.

For a long time, electron-electron interaction due to electron correlation has been assumed to determine the low energy electronic structure. However recently Sawatzhy et al[5] and Fujimori et al[6] proposed, based on experimental results obtained on NiO, another electron-electron interaction that also plays an important role - the charge transfer energy (Δ).

It is defined as

$$\Delta = E_I\left(d^{n+1}\underline{L}\right) - E_A\left(d^n\right) \qquad (2)$$

where d is the 3d state electron, $\underline{L}$ is the energy to transport an electron from one ion to another, E_I is the ionization energy and E_A is the electron affinity. In the case where Δ is dominant over U, such as for $NiSe_2$, the influence of the process involving the transport of an electron from Se^- to the Ni^{2+} 3d state ($d^n \rightarrow d^{n+1}\underline{L}$) as shown in Figure 4a, is even lower in energy than U between the 3d-3d state. When Δ is favored over U, the energy gap formed at the 3d band in Ni^{2+} due to electron correlation is removed. Therefore with partially filled 3d electrons and no energy gap, the physical/electronic properties would be metallic as observed in $NiSe_2$.

3

Based on the relative values of U, Δ, and W (the dispersion width of the electron bands involved), a classification scheme, shown in Figure 5, has been introduced by Zaanen et al[7] that can be used to explain the material properties of $NiSe_2$ and NiS_2 by considering the competition between W, Δ, and U. In the case where U is larger than Δ, which in itself is larger than W, the open 3d band is separated by an energy gap. The physical/electronic property, as shown in Figure 3b, is insulating as observed in NiS_2. If U is smaller than Δ, which in itself is smaller than W, there is no energy gap. With partial filled 3d electrons as shown in Figure 3a, metallic properties are predicted as observed in $NiSe_2$.

The insulating and metallic characteristic observed in NiS_2 and $NiSe_2$ are not only of intrinsic interest. They can be used to provide experimental inputs for a theoretical understanding of the effect of strongly interacting electrons to induce metal to insulator transition (MIT) when BT is no longer applicable. As noted earlier, NiS_2 has insulating property due to the 3d band being split by strong on-site Columbic repulsion. The investigation led by the DuPont group[8-10] has found that the insulating property of NiS_2, with the same pyrite structure as $NiSe_2$, can transition to metallic behavior by alloying with Se to form a mixed crystal of $NiS_{2-x}Se_x$, where x is the Se composition. Depending on temperature, $NiS_{2-x}Se_x$ can magnetically order to paramagnetic, anti-paramagnetic, ferromagnetic, or anti-ferromagnetic. These properties, and the focus of this thesis, have important applications in understanding the strength and nature of electron interaction and how strongly interacting electrons can induce MIT.

1.2 Overview of $NiS_{2-x}Se_x$

$NiS_{2-x}Se_x$ has been investigated by many over the years - initially by the DuPont group[8-10] in the period from 1968 to 1973, Jarrett et al (1973)[11], Krill et al[12]

(1976), Mabatah et al[13] (1980), Kwizera et al[14] (1981) and Matsuura et al[15] (1997), and a comprehensive review by Wilson[1-2] (1931) and Honig[16] (1998).

The pyrite structure $NiS_{2-x}Se_x$ with PA3 space group is an excellent system to understand electron interaction and MIT. This is because of its remarkable changes (i.e., phase transition) in electrical property from insulator to metallic by alterations in the anion composition with either sulfur (S) or selenium (Se) or temperature. $NiS_{2-x}Se_x$ shows no apparent change in structural symmetry at the metal to insulator transition or by modifying the S and Se composition as confirmed by Jarrett et al[11] by x-ray diffraction experiments. The structure as shown in Figure 6 is a face-centered cubic lattice with Ni^{2+} ions occupying octahedral symmetry and S/Se atoms occupying tetrahedral symmetry. Since $NiS_{2-x}Se_x$ is cubic, the lattice parameters are equal (i.e., a=b=c).

Investigation of the electron interaction and MIT in solid using this system is possible because NiS_2 and $NiSe_2$ are good insulator and metallic respectively. Mixture of these two components and changes in temperature would result in a continuous changeover from one regime to another. This is possible because NiS_2' electronic structure is insulating but becomes metallic upon mixing with $NiSe_2$ to become a mixed crystal $NiS_{2-x}Se_x$[8-10] where x is the Se composition. When x is between 0 < x < 0.38, the material is an insulating semiconductor and possesses anti-ferromagnetic ordering between $T_{Néel}$ = 35 – 45 K[5] and paramagnetic when $T_{Néel}$ > 45 K[5]. As x is increased between 0.38 < x < 0.55, there is an insulator to metal transition that is anti-ferromagnetic at low temperature less than 45K and paramagnetic at high temperature greater than 45K. Investigation by Gautier et al[17] reported in the vicinity of x = 0.43, a MIT transition is induced by temperature. Further work by Thio et al[18] indicated that there is evidence of anti-ferromagnetic correlations on both sides of MIT. Recent

work by Matsuura et al[15] (1997) using ARPES technique confirmed results from the above references 5, 17, and 18.

When x is further increased between 0.55 < x < 2, the material is predominantly metallic and, depending on the temperature, can be either paramagnetic or anti-ferromagnetic as shown from its phase diagram in Figure 7, which was obtained from conductivity and magnetic susceptibility data[16]. In summary, with increase in x, the material transition from insulating to metallic and magnetic ordering from anti-ferromagnetic to paramagnetic as temperature is increased.

From the phase diagram shown in Figure 7, there are different regions to study MIT and the types of magnetic ordering such as anti-ferromagnetic, a paramagnetic, or ferromagnetic metal or insulator by careful selection of composition (x) and temperature. In this work, the composition was fixed at x = 0.62 for $NiS_{2-x}Se_x$ and temperature varied. X-ray adsorption spectroscopy (XAS) technique is used to study the changes in atomic distances as $NiS_{2-x}Se_x$ (x=0.62) undergoes AFM to WFI transition as the temperature increased from 0K to 70K, which exists according to the phase diagram for x = 0.62 at ~ 18 K[16].

1.3 Thesis Statement

XAS measurements of absorbance versus temperature were conducted to detect changes in the absorbance at the Ni and Se K Edges as amorphous powder $NiS_{2-x}Se_x$ (x=0.62) undergoes AF metal to WF insulator phase transition. Absorbance versus energy in the temperature range from 0 to 70K indicates an increase in atomic absorption above the Se K Edge in the 18 to 20K temperature range and no change in the Ni K Edge. Extended x-ray adsorption fine structure spectroscopy (EXAFS) analysis confirms that as the temperature decreases below $T_{Néel}$, the relaxation time for the final states in the EXAFS region increases as the

WFI order increases. X-ray temperature difference adsorption spectroscopy (XTDAS) data correlates well with EXAFS analysis and the material phase transition diagram for AF metal to WF insulator transition, which suggests that WFI is more ordered in the insulator state than AF metal state.

1.4 X-ray Absorption Fine Structure Spectroscopy (EXAFS)

The Extended X-ray Absorption Fine Structure (EXAFS) refers to oscillations of X-ray absorption coefficient (μ) beyond the threshold of an absorption Edge for atoms either in a molecule or embedded in a condensed phase as X-rays pass through a material. When the X-ray photon energy (E) is tuned to the binding energy of an atom, an abrupt increase in the absorption coefficient occurs. These energies are referred to as absorption Edges and correspond to the ejection of a photoelectron from an excited atom, which occurs when the energy of the incident X-ray is equal to the threshold energy required to eject an electron. With increasing energy away from the absorption Edge, simple X-ray absorption models predict a gradual monotonic decrease in the absorption coefficient. This behavior is observed in spectra of isolated atoms but not for atoms in a molecule or embedded in a condensed phase. For cases of non-isolated atoms, Kronig[19] in 1932 introduced a single scattering short range order theory (SRO) to explain modulation in μ as being due to the modification of the final state of the photoelectron by the presence of neighboring atoms around the excited atom. The modulation in μ as observed in a XAS spectrum came to be known as the EXAFS region.

EXAFS has been known for a long time and Kronig's[19] work has paved the path toward the understanding of such a method but its application for structure determination was only developed in the last two decades. A major reason for the confusion was the lack of detailed agreement between theory and experiment. In spite of this confusion, there were some applications made of

EXAFS as an experimental tool. Chemical bond information using near Edge structure was obtained by Mitchell and Beaman[20] (1952) and van Nordstrand[21] (1960). Nearest neighbor distance determinations were made by Lytle[22-23] (1965, 1966) and Levy[24] (1965). However, these efforts did not attract general attention because of the confusion surrounding the subject. The situation changed when Sayers, Sten and Lytle[25] (1971) pointed out, based on a theoretical expression of the EXAFS (1970)[26], which has since become the accepted modern form, that a Fourier transform of the EXAFS with respect to the photoelectron wave number should peak at distances corresponding to nearest neighbor coordination shells of atoms. Instead of comparing EXAFS measurements to theoretical calculations based on atomic parameters whose values were difficult to calculate, it is now possible to use EXAFS to extract structure information directly and to determine experimentally all of the required atomic parameters.

In summary, EXAFS is related to the radial distribution of atoms in the sample. By analyzing the frequency and amplitude of the oscillation of a XAS absorption spectrum, information about the local environment of the absorbing element at or close to its phase transition can be derived.

Qualitative rationalization of the absence and presence of EXAFS and its use for structural information is pictorially described as follows: For a mono-atomic gas with no neighboring atoms, the ejection of a photoelectron, by absorption of a X-ray photon, will travel as a spherical wave with a wavelength λ = 2pi/k where k is expressed as:

$$k = \sqrt{\frac{2m}{\hbar^2}(E - E_o)} \qquad (3)$$

The $(E-E_o)$ term is the energy of the ejected photoelectron of that particular absorption Edge. The μ vs E curve follows the usual smooth decay. In the presence of neighboring atoms, the outgoing photoelectron can be backscattered from the neighboring atoms thereby producing an incoming wave which can

interfere either constructively or destructively with the outgoing wave near the origin. The result of the interaction is the oscillatory behavior of the absorption rate and the generation of the EXAFS signal. The amplitude and frequency of EXAFS depend on the type and bonding of the neighboring atoms and their distances away from the excited atom.

The simple picture of EXAFS was formulated into the Short Range Order (SRO) theory presented by Kronig[19] in 1932. For reasonably high energy and moderate thermal or static disorders, the oscillation of the absorption rate, $\chi(E)$, in EXAFS, normalized to the background absorption (μ_o) is given by

$$\chi(E) = \frac{\mu(E) - \mu_o(E)}{\mu_o(E)} \tag{4}$$

To relate $\chi(E)$ to structural parameters, the energy E is converted into the photoelectron wavevector unit (k) via equation 3. This transformation of $\chi(E)$ in E space gives rise to $\chi(k)$ in k space:

$$\chi(k) = \sum_j N_j S_i(k) F_j(k) e^{-2\sigma_j^2 k^2} e^{\frac{-2r_j}{\lambda(k)}} \frac{Sin(2kr_j + \phi(k))}{2kr_j^2} \tag{5}$$

where $F_j(k)$ is the backscattering amplitude from each of the N_j neighboring atoms of the Jth type with a Debye-Waller factor (σ_j) - accounting for thermal vibration and static disorder (S) and at a distance (r_j) away. $\phi_j(k)$ is the total phase shift experienced by the photoelectron as it backscatters from neighboring atoms to the excited atom. The term $e^{(-2r_j/\lambda)}$ is due to inelastic lost in the scattering process – mainly due to neighboring atoms and the medium in between with wavelength (λ) being the electron mean free path.

Each EXAFS wave is determined by the backscattering amplitude $(N_j F_j(k))$, modified by the reduction factors $(S_i(k))$, $e^{(-2\sigma 2jk2)}$, $e^{(-2rj/\lambda)}$, the $1/kr_j^2$ distance dependence and the sinusoidal oscillation which is a function of inter-atomic distances $(2kr_j)$ and the phase shift $(\phi_j(k))$. The amplitude function $F_b(k)$ depends

only on the type of the backscatters while the phase function contains contributions from both the excited atom and the back-scatterer. In addition, the Debye-Waller factor (σ) plays an important role in EXAFS spectroscopy. σ contains important both structural and chemical information which is otherwise difficult to obtain, yet it comes as a bonus in the EXAFS determination of inter-atomic distance. Since atoms are not stationary, thermal vibration will smear out the EXAFS oscillation and in the harmonic approximation this can be accounted for by a Debye-Waller type term $e^{(-2\sigma^2 k^2)}$. The Debye-Waller factor as determined by EXAFS is different from that implied by conventional crystallography in that σ_{EXAFS} refers to the root-mean-square relative displacement along the bond direction and not the absolute root-mean-square displacement of individual atoms. For the first shell, the motions are significantly correlated whereas for higher shells the correlations are greatly reduced.

1.5 EXAFS and X-ray Source Overview

The progression of investigations and discoveries of EXAFS over the years by scientists has resulted in its establishment as a practical structural tool and more importantly as a science. The first experimental detection of EXAFS past the absorption Edges was discovered by Fricke[27] and Hertz[28] in 1920. Twelve years later, Kronig[19] presented his SRO theory to understand EXAFS. It was not until 1971 that it was realized with the work by Sayers, Sten and Lytle[25-26] that structural determination can be achieved by Fourier transformation of the EXAFS signal. With increased availability of synchrotron radiation sources of X-rays several years after the potential of EXAFS was first shown, the accessibility of EXAFS measurements for structural determination was greatly enhanced. Because synchrotron sources typically have X-ray intensities more than three orders of magnitude greater in the continuum energies than the standard x-ray

tube sources as discussed by Lytle et al[29] in 1975, the time for measuring a spectrum for concentrated samples dropped from the order of weeks to minutes.

2. EXPERIMENTAL

There are several approaches of synthesizing $NiS_{2-x}Se_x$ with the desired stoichiometry. One approach is through casting where the ceramic technique. $NiS_{2-x}Se_x$ is synthesized by reacting Ni, Se, and S in appropriate amounts at elevated temperature, follow by grinding and firing to achieve the desired stoichiometry. Another alternative approach is the chemical vapor transport technique by Bither et al[30]. In this research, the group of Honig at Purdue University, using the ceramic technique, supplied sample of $NiS_{1.38}Se_{62}$ for XAS analysis at Stanford Synchrotron Research Laboratory (SSRL).

2.1 X-ray Source

A strong X-ray source such as synchrotron radiation is required to produce features sufficiently intense to be analyzed since oscillations in μ, generated in the post Edge or EXAFS region, are small compared to the absorption resulting from the electron ejection. Because of the small number of synchrotron radiation sources and closest location available, the Acrivos group conducts all X-ray Absorption Spectroscopy (XAS) research at Stanford Synchrotron Research Laboratory (SSRL). Details on synchrotron radiation and its applications can be found in the references[31, 32]. This work is supported in part by the National Science Foundation (NSF) and Department of Energy (DOE).

2.2 Procedures for XAS Experiment and Data Acquisition

A two silicon crystal monochromator is used to select X-ray energies specific to an element in the material for the analysis. This beam is projected through a series of chambers equipped with current-sensing electronics and an applied voltage that measures the intensity of the incident beam flux after each absorption event. The beam flux's path as shown in Figure 8 is as follow: I_0, the incident x-ray beam after passing through the slit, I_1, after sample absorption,

and I_2, after reference sample absorption. Each chamber is respectively filled with helium (He) for I_0, elemental nitrogen (N_2) for I_1, and argon (Ar) gas for I_2. When the incident beam passes through each chamber, the gases are ionized and a current is created. Since the current is proportional to the intensity of the incident beam flux, data can be collected by XAS Collect software at SSRL for XAS analysis. The data run files at Se and Ni K Edges are shown in Table 1 and 2. An Oxford Instruments Cryostat is used to control the sample temperature and a Strawberry Tree Data Acquisition card™ connected to a computer is used to collect the temperature data. A plot of temperature as a function of time for both the Ni and Se data collection at the K Edge is shown in Figure 9.

2.3 Sample and Mounting for XAS Experiment

The quality of XAS data collection depends on the ability to achieve high signal to noise ratio (SNR). One approach for optimal SNR is to tune the sample absorbance to change the incident beam flux or absorbance by 90% at the absorption Edge. This is accomplished by diluting $NiS_{1.38}Se_{62}$ with an inert sample with low mass absorption coefficient (α) such as boron nitride (BN). The proportion of $NiS_{1.38}Se_{62}$ and BN mixture to achieve the desire absorption is determined from the Beer-Lambert Law equation in term of α as follows:

$$A = \ln(I_0/I) = t\,\mu = -\alpha c t \qquad (6)$$

where A is the molar absorption coefficient which is directly proportional to the product of t (sample's thickness) and μ (linear absorption coefficient) and $\alpha c t$, where α is the mass absorption coefficient or cross section, c is the concentration of the sample and t is the sample thickness. At the absorption Edge, the change (Δ) in absorbance can be accounted by

modifying equation 6 as follows:

$$x \, \Delta\mu = x_1 \, \Delta\mu_1 = \Delta\alpha_1 \, d_1 \, x_1 \qquad (7)$$

The effective contribution to the total absorption is from the absorber, such as Ni or Se, and the background such as BN. Since the total absorption is unity for an optimal signal to noise ratio, the amount of BN and $NiS_{1.38}Se_{62}$ needed to give the optimal SNR using Se at the K Edge as the strong absorber is calculated by modifying equation 7 as follows:

$$d_1 x_1 = 1/(114.1) = 0.000876 \text{ g/cm}^2 \qquad (8)$$

Since the area of the sample holder is 0.4 X 1.8 cm^2, the amount of $NiS_{1.38}Se_{62}$ is determined by:

$$\text{Weight}_{NiS2\text{-}xSex} = (0.00876 \text{ g/cm}^2)(0.4 \text{ X } 1.8 \text{ cm}^2) = 0.00631 \text{ g} \qquad (9)$$

The amount of BN to dilute $NiS_{1.38}Se_{62}$ with a density of 2.25 g/cm^3 is determined as follows:

$$\text{Weight}_{BN} = (2.25 \text{ g/cm}^3)(0.2 \text{ X } 0.4 \text{ X } 1.8 \text{ cm}^3) = 0.324 \text{ g} \qquad (10)$$

The measured amounts of $NiS_{1.38}Se_{62}$ and BN are mixed, grinded, transferred and filled in the slit of the sample holder and sealed with para-film that is transparent to x-ray. The area around the slit of the sample holder is sealed with lead to prevent absorption from sample holder. After the sample is prepared, it is transferred to the XAS apparatus for analysis. The $NiS_{1.38}Se_{62}$ film is mounted to a sample holder, cooled in liquid nitrogen and inserted into Oxford Dewar and Goniometer. Helium is purged into the chamber three times to remove moisture that can condense on the sample holder during transferring the sample to the Oxford Dewar. The sample is then aligned in the XYZ direction to maximize the

incident flux beam through the sample. From the phase diagram[16], the data is obtained for $NiS_{1.38}Se_{62}$ at or close to the phase transition temperature (T_{Neel}) for AF metal to WF insulator transition.

2.4 Correlating XAS Data at Ni and Se K Edges to Temperature

XAS data and temperature data are collected on two separate computers, where the first computer records XAS versus energy (C1) and the second computer records temperature (C2). Date and time when the data was generated are also recorded on both the C1 and C2 computers. By obtaining the date and time, it is then possible to correlate the temperature scan to the XAS data of each run using the following procedure: to determine the temperature for each file, the temperature scans need to be analyzed to show date, time, and corresponding temperature. The method by Strawberry Tree for temperature collection is unique that it only records date, temperature and time increment at selected duration (60 second interval). This is not the actual time as shown in Table 3 for Se K Edge files. To correlate temperature to XAS data, the initial time is first converted from 12 hour to 24 hour timeframe then the delay time is added to the initial time for each temperature recorded. Since the delay time is shorter than the duration to complete a XAS collection, the temperature for each XAS run is determined by averaging the temperature fluctuation during the duration of the XAS scan. The temperature range for each scan for Ni K Edge file is shown in Table 4. The average temperature range for Ni K Edge is 61.8 K to 1K with 15.3% temperature fluctuation (high-low/2mean). For Se K Edge, as shown in Table 5, the temperature range is 14.1K to 80.6K with 15.8% temperature fluctuation. For each XAS scan used for further analysis, temperature fluctuation is limited to 8% – else the XAS scan is rejected. At the end, the XAS scan is matched to the corresponding temperature scan then sorted from lowest to

highest temperature for EXAFSPAK analysis. A plot of temperature versus run number for XAS acquisition at Ni and Se K Edges is shown in Figure 9.

2.5 Overview of XAS Absorption Spectrum

According to the nature of the final states of photoelectrons excited from core levels and the extent of their interaction with neighboring atoms, a typical XAS absorption spectrum consists of four regions as shown in Figure 10: Pre-Edge, Edge, XANES (X-ray Absorption Near Edge Structure), and EXAFS (Extended X-ray Absorption Fine Structure). The pre-Edge is essentially the background in the XAS spectrum. The Edge is the point when the energy of the monochromator is adjusted to match the binding energy of the absorber to promote an electron to the continuum. As the electron is ejected out of the absorber, it will scatter from neighboring atoms, which is shown in the XANES and EXAFS regions. XANES region is predominated by atoms closest to the absorber while EXAFS regions occurs 50 eV beyond the Edge or 10A away.

2.6 XAS Data Analysis

There are two major approaches to EXAFS data analysis: the exact Fourier transform (FT) and the curve fitting (CT) techniques as shown in Figure 11. In either method, the μ vs E data obtained from the data collection is converted into $\chi(k)$ vs k via equation 4 and 5. $\chi(k)$ is then multiplied by k^3 so as to compensate for the diminishing amplitudes at high k values to give $k^3\chi(k)$. One could multiply $\chi(k)$ by some power of k to give $k^n\chi(k)$ before fitting so as to emphasize different k regions (the higher the n values, the more weighting is the higher k regions) or simply apply a weighting scheme as a function of k. The resulting data, in unit of $k^3\chi(k)$, is inserted into FT or CT for further analysis.

The XAS data will be analyzed using EXAFSPAK™ developed by Graham George[31] at SSRL. While both FT and CT will be used to analyze the $NiS_{2-x}Se_x$ data

at the Ni and Se K Edges only, the CT method will be discussed in this section. The FT method will be discussed in section 3.3. Before analyzing the data with CT, the raw data needs to be filtered (Figure 11, Data reduction) and the resulting EXAFS electron waves extracted prior to subjection to fast Fourier transform (FFT) for Fourier filtering. The FFT technique will then be used to convert the EXAFS spectrum from the frequency dimension to the distance dimension. The CT method along with a phenomenological structure model of $NiS_{2-x}Se_x$ will be used to generate the best fit from the EXAFS spectrum produced from FFT.

To filter the raw EXAFS data, EXAFSPAK™ offers three sequential mathematical operations such as removing glitches, subtracting the background, and finally extracting EXAFS. EXAFSPAK™ has a function to pinpoint glitches due to crystal defects in the monochromator and easily remove them from the XAS spectrum. The background is removed by first fitting the raw data to a polynomial function then subtracting the function from the raw data. A spline function is performed on the data with the background removed. Spline function (Figure 11, EXAFS extraction) is a polynomial function that is fitted to the EXAFS region and later used to create the EXAFS spectrum for Fourier transform. Three functions such as raw pre-Edge data (μ_{exp}), spline (μ_s) and a correction function (μ_{vic}) are used to generate the EXAFS spectrum after data reduction with the following equation:

$$\chi(k) = (\mu_{exp} - \mu_s) / \mu_{vic} \qquad (11)$$

The correction function is used to account for distortion in the data that can potentially occur due to subtraction of the pre-Edge data. The expression for the correction function is:

$$\mu_{vic} = C_{vic} \lambda^3 + D_{vic} \lambda^4 \qquad (12)$$

where λ is the x-ray wavelength and C_{vic} and D_{vic} are the coefficients, which are unique to each element and absorption Edge. The filtered EXAFS data is shown in Figure 12 and the EXAFS removed from the filtered data is shown in Figure 13 for the Ni and Se at the k Edge.

Fast Fourier Transform (FFT) (Figure 11, Fourier Transform) is used to Fourier transform of the filtered EXAFS in unit of k3χ(k) in momentum (k) distance space over the finite k range k_{min} to k_{max} to give the radial distribution function $\rho(r')$ in distance r space using the following equation:

$$\rho(r') = \frac{1}{(2\pi)^{1/2}} \int_{k\,min}^{k\,max} k^n \chi(k) e^{i2kr} dk \qquad (13)$$

The aim of FFT is to do Fourier filtering. It involves Fourier transforming $k^3\chi(k)$ data into the distance space, selecting the distance range of interest with some smooth window, and back transforming the data to k space. The resulting 'filtered' EXAFS spectrum $k^3\chi(k)$ as shown in Figure 14 can then be fitted with a Marquardt algorithm in OPT-EXAFSPAK™ to get the coordination shell and distance information from the FT-EXAFS data.

A model compounds for $NiS_{2-x}Se_x$ system generated in T. Norman's[32] thesis work will be used to generate the initial inter-atomic distances and coordination numbers guesses for the best fit. An outline of the approach for data analysis and curve fitting for Ni and Se K Edge files is shown in Figure 11.

2.7 Determination of Atomic Distances of S, Ni, and Se in $NiS_{2-x}Se_x$

To use the CT method, generation of a model compound of $NiS_{2-x}Se_x$ is required as outlined in Figure 11. Work by Xiaoqiang[33] has determined that $NiS_{2-x}Se_x$ obeys Vegard's law. According to this law, the unit cell dimensions of a mixed crystal vary linearly with composition. A plot of Vegard's Law for $NiS_{2-x}Se_x$ provided by Norman[31] is shown in Figure 15. The slope as determined

from the plot is 0.1359 Å/Se composition. Since the unit cell dimensions varies linearly with composition, the lattice parameter for a composition of x = 0.62 for the $NiS_{2-x}Se_x$ sample is 5.7705 Å. Because $NiS_{2-x}Se_x$ follows the PA3 space group where the lattice parameters follows a cubic structure (a=b=c), the unit cell dimension for $NiS_{2-x}Se_x$ (when x = 0.62) can be constructed by multiplying x, y, and z coordinates for a PA3 space group by the lattice parameter as shown in Table 6. The distances between the atoms can then be calculated using the distance equation as follows:

$$d = \left[(x_a - x_b)^2 + (y_a - y_b)^2 + (z_a - z_b)^2 \right]^{1/2} \quad (14)$$

The resulting distances of Se and Ni atoms to each other and to S are shown in Table 7. As shown in Figure 16, these distance values are used to set up a phenomenological structural model for generating the initial inter-atomic distances and coordination number guesses for the EXAFS fitting (OPT) routine provided by EXAFSPAK™. OPT uses a derivative method as shown to search the minimum points in the parameter-space.

$$\chi(k) = S_o^2 \Sigma \left[N_i S_i(k, R_i) F_i(k, R_i) \right] / kR_i^2 = *$$
$$\exp \left[-2R_i / \lambda(k, R_i) \right] * \exp (-2\sigma_i^2 k^2) *$$
$$\sin \left[2kR_i + \phi_c(k) \right] \quad (15)$$

It will first calculate the first derivative of the complete EXAFS function to each fitting variable and using them to construct a parameter-derivative matrix. By solving the inverse-matrix of this derivative matrix, the program will determine the next search step toward the local/global minimum point. The result of FT-EXAFS curve fit is shown in Figure 17 for both Se and Ni K Edges using the largest atomic number as the backscatterer. The distance information from FT-EXAFS curve fit is provided in terms of R+Δ. R is determined by subtracting the

19

Se-Se, Se-S, Ni-Se, Ni-S, and Ni-Ni distance calculated from the model (R+Δ) at the highest temperature data for Ni and Se at k Edges.

3. RESULTS

3.1 Ni K Edge Data

Figures 18, 19, and 20 show multiple superimposed XAS scans of x-ray absorption versus energy at the Ni K Edge for a temperature range from 0.5 K to 62 K. Since the final state of the electron is influenced by neighboring atoms from the absorber, changes in the EXAFS spectrum at different temperatures would indicate changes to the atoms in $NiS_{1.38}Se_{0.62}$. Since the pre-peak intensity and the position of the peak did not change through the measured temperature range as shown in Figure 18 and 20, this indicates that both coordination number and valence did not change with temperature. In addition, since there was no change in the XAS slope, the relaxation time for the final states was correspondingly unchanged for the measured temperature range.

The Ni distance to other atoms obtained from EXAFS analysis indicated that Ni-Ni, Ni-Se and Ni-S bond distances all fluctuated with temperature as shown in Figure 21, 22, and 23 respectively. As the temperature was increased from 0.5K to 20 K, both Ni-S and Ni-Se distances increased: Ni-S distance increased from 3.1302 ± 0.010 Å at 0.5 K to a maximum peak of 3.1351 ± 0.011 Å at 20 K while the Ni-Se distance increased from 3.4831 ± 0.011 Å for Ni-Se to 3.4870 ± 0.010 Å. The Ni-Ni distance on the other hand decreased from 4.1370 ± 0.009 Å at 0.5K to a minimal of 4.1320 ± 0.011 Å at 20 K. From 20 to 45 K temperature range, Ni-S and Ni-Se distances both decreased to a minimum from 3.124 ± 0.011 Å to 3.4779 ± 0.010 Å, respectively, while Ni-Ni distance remained constant at temperature higher than 20 K. As the temperature was further increased, Ni-S and Ni-Se distances gradually increased back to their initial values at 0.5K and Ni-Ni distance also goes back to its initial value.

3.2 Se K Edge Data

Since the magnitude of the absorption peaks in the XAS spectrum is a function of the number of atoms at the peak position, changes in peak intensity and position correlate to changes in the valence, coordination number or crystal field parameters at the measured temperature range. Figure 24, 25 and 26 show superimposed plot of multiple XAS scans of x-ray absorption versus energy at the Se k Edge for a temperature range from 2 to 70 K. The Se K Edge results are much different from the XAS spectrum acquired at the Ni K Edge at the similar temperature range. Both pre-peak intensity and peak position changed with temperature in the temperature range from 18 to 23 K then remained constant at temperatures higher than 23 K. In addition, as seen from the figures (24, 26 and especially 25), the XAS absorption spectrum varied with temperature beyond the K Edge for Se, which indicated that the environment or more specifically the distances of neighboring atoms, or backscatterers, was changing as a function of the measured temperature range.

The Se distance to other atoms obtained from EXAFS analysis indicated that Se-Ni, Se-Se and Se-S bond distances all fluctuated with similar systematic trend at the measured temperature range from 2 to 70 K as shown in Figure 27, 28, and 29 respectively. As the temperature was increased from 0 to 18K, Se-S, Se-Se and Se-Ni distances expanded from 3.3231 ± 0.010 Å to 3.3451 ± 0.010 Å for Se-Ni, 3.6951 ± 0.010 Å to 3.7079 ± 0.010 Å for Se-S and 3.6550 ± 0.010 Å to 3.6740 ± 0.010 Å for Se-Se. When the temperature was further increased from 18 to 25K, Se-S, Se-Se and Se-Ni distances compressed to 3.3074 ± 0.010 Å for Se-Ni, 3.6814 ± 0.010 Å for Se-S and 3.6814 ± 0.010 Å for Se-Se. At temperature higher than 25K of the measured temperature range, Se-S, Se-Se and Se-Ni distances remained constant. Distances values from both Ni and Se k Edges data show direct correlation. As the temperature was increased, both Ni-Se and Se-Ni distances from Ni and Se k Edge scans increased in the temperature range from 18 to 20K.

3.3 X-ray Temperature Difference Absorption Spectrum

The dependency of structure change to temperature can be determined from X-ray temperature difference absorption spectrum (XTDAS)[34] analysis by taking the difference of the absorption spectrum at specified temperature relative to the normal state (ST) as shown:

$$XTDAS = A(T) - A(T_{ST})$$ (16)

where A(T) is the absorption at the specified temperature T and $A(T_{ST})$ is the temperature of the normal state. The net result, XTDAS, is the absorption due to the perturbation as shown in Figure 30.

EXAFS in XAS measurement, in general, is the sum of electron waves excited from the absorbing atoms and interaction from neighboring atoms in a sample. When the sample is perturbed by pressure or temperature, the electron waves will further be altered producing a different EXAFS spectrum - $EXAFS_{perturbed}$. The effect of the perturbation on the electron waves can be determined by applying the XTDAS method. The result of subtracting an EXAFS spectrum of a specific state from the EXAFS spectrum of a perturbed state is a net EXAFS spectrum due only to the perturbation by pressure or temperature - in our case temperature.

The following information can be provided from XTDAS analysis: first if the perturbed spectrum and specific spectrum are identical, the slope of XTDAS will be equal to zero. In this case there is no perturbation effect on EXAFS. Secondly if either or both the band structure or relaxation time changes then XTDAS' corresponding line shape and slope will change. Thirdly although oscillation in XTDAS can result from other factors such as Debye-Waller factor (σ) or constructive canceling of EXAFS of different intensities, XTDAS does offer information on the electron density around the absorbing atom changes without changes in the bond angle or length by the observance of oscillation. And finally

changes in XTDAS' slope can reflect the increase in the excited state's lifetime and band structure as the temperature is varies.

The MIT in $NiS_{2-x}Se_x$ was studied at the Ni and Se K Edges at temperature ranging from 2 to 70 K. Figures 18 and 19 show the absorption versus temperature plot at the Ni K Edge. As the temperature was increased from 1K to 62 K, EXAFS did not show any observable fluctuation. XTDAS data indicates that at the temperature lower than 7 K, perturbation effect was negligible; about ~ 7 K, band structure or relaxation time began to change; and higher than 7 K the changes were more dramatic as shown in Figure 31 and magnified in Figure 32. Debye-Wall plot shows σ (sigma) to be stable at higher temperature but fluctuates at temperature lower than 20 K as shown in Figure 33. Absorption versus temperature plot at the Se K Edge, on the other hand, shows two populations of EXAFS as a function of temperature. EXAFS shifted to higher absorption were from the temperature range of 18 to 20K while the lower absorption EXAFS were from the temperature range outside the 18 to 20K as shown in Figure 24 and 25. XTDAS shown in Figure 34 indicates that there was fluctuation in EXAFS or more specifically, the sum of electron waves. In the temperature range from 18 through 20 K, changes in the XTDAS slope reflected the increase in relaxation time and change in the band structure. The Debye-Waller plot shows similar trend as XTDAS for this temperature range as shown in Figure 35 at the Se K Edge. The Debye-Waller was stable at higher temperatures but fluctuated at 18 through 20 K temperature range.

4. DISCUSSION

The temperature-induced metal to insulator transition in $NiS_{2-x}Se_x$ for $x = 0.62$ according to the Mott-Hubbard model[3-4] is due to the progressive change in electron correlation (U). Moreover, work by Mott[3] emphasize the U is increased when the atomic distances are large and vice versa. According to the generalized classification scheme introduced by Zaaene, Sawatzky, and Allen[7], electron correlation can be viewed as the competition between W, Δ and U. The stronger of either W and Δ or U will determine the electronic property of $NiS_{2-x}Se_x$. For example if the W and Δ terms dominates over U and Δ is less than W, the materials is metallic. If U dominates over Δ and W, the material will be insulating.

EXAFS technique can be used to determine the strength of electron correlation and atomic distance changes as a function of temperature at or in the vicinity of the magnetic metal to insulator transition to further understand MIT. The advantage of using this technique is the ability to probe the interatomic distance of atoms surrounding each species of atom in the material simply by tuning the x-ray energy to the absorption Edge of that element. Changes in the electron density or interatomic distance due to temperature changes will correspondingly result in the change in EXAFS. Therefore by varying the temperature and examining the corresponding EXAFS spectrum and XTDAS data, this approach can be used to characterize the effect of electron correlation and changes in atomic distances during the magnetic metal to insulator transition.

Application of XAS, EXAFS, and XTDAS analysis at both Ni and Se K Edges of $NiS_{1.48}Se_{0.62}$ in the temperature range from 70 to 2 K suggests a phase transition from an anti-ferromagnetic metal to a weak ferromagnetic insulator at the 18 K temperature limit.

As shown in Figure 36, support for this conclusion is from the excellent correlation between the phase diagram[16] and XAS data obtained at the Se k Edge, which confirmed $NiS_{1.48}Se_{0.62}$ transition from AF metal to WF insulator. As the temperature was lower from 70 to 2 K, the Ni, S and Se bond distances as determined from OPT and the phase diagram, were changing as follows: at 70 K, $NiS_{1.48}Se_{0.62}$ is an anti-ferromagnetic metal as indicated from the phase diagram[16]. As the temperature was lowered past 40 K, the plots in Figures 21, 22, and 23 of EXAFS analysis at the Ni K Edge indicated that the Ni-Se and Ni-S bonds began to expand while the Ni-Ni bond compressed and reached a maximum distance at 18 K where the material became a weak ferromagnetic insulator. As the temperature was further lowered, the opposite effect occurred whereby the Ni-Se and Ni-S bonds began to compress while the Ni-Ni bond compressed. EXAFS analysis at the Se K Edge, similarly, indicated the distances of Se to Ni, Se and S tend to compress at temperature higher or lower than 18 K but expand at the metal phase transition ~ 18 K as shown in Figure 27, 28, and 29. These results correlated well with the distance data analyzed at the Ni K Edge for the Ni-S and Ni-Se bonds.

EXAFS analysis at both the Ni and Se K Edges correlated with the classification scheme introduced by Zaaene, Sawatzky, and Allen[7] for predicting material properties of $NiS_{2-x}Se_x$ for x = 0.62 in term of W, Δ and U. At high temperature, the W and Δ terms dominates over U and Δ is less than W, therefore $NiS_{1.38}Se_{0.62}$ is metallic. As the sample's temperature decreased below 18 K, the contribution of W and Δ diminished while the U term dominated. The net effect of increasing U was $NiS_{1.38}Se_{0.62}$ becoming insulating.

Multiple superimposing XAS scans of x-ray absorption (Abs) versus energy at the Ni and Se k Edge for a temperature range from 2 to 70 K are shown in Figure 18 and 24 and their respected magnified EXAFS in Figure 19 and 25. For a plot of absorption versus temperature, the present of changes in the XAS

slope in the post Edge region would indicate a change in the relaxation time of the final states ($\tau_{final\ states}$). Observation on the XAS spectrum at Se K Edge showed two distinctive EXAFS spectrums having slopes of -4.5x10^{-4}/eV and 1.5x10^{-4}/eV with 1.5x10^{-4}/eV having an increased atomic absorption above the Se k Edge as shown in Figure 24. The analysis by Acrivos et al[34] on superconductors and MIT materials indicates that the changes in the relaxation time of the final states is due to fluctuations caused by changes in the atomic structure and electron density as a function of temperature of neighboring atoms near the absorber during the onset of a phase transition.

According to Mott's model[3,32,34], the changes in $\tau_{final\ states}$ were due to changes in the anti-ferromagnetic (AF) to weak ferromagnetic (WF) ordering as a function of temperature. As the temperature was decreased to the metal to insulator transition, the Se-S, Se-S, and Se-Ni atomic bond distances increased. This resulted in a cascade event where both the electron density and the relaxation time increased. Above $T_{Néel}$, the AF ordering and $\tau_{final\ states}$ decreased but as the temperature was lower to $T_{Néel}$ AF to WF ordering and $\tau_{final\ states}$ increased. In the case of $NiS_{1.48}Se_{0.62}$, the increase of atomic absorption of 1.5x10^{-4}/eV can be explained by an increase in AF to WF ordering and $\tau_{final\ states}$. These observations indicate that the atomic absorption is very sensitive to changes in $\tau_{final\ states}$. Since τ_{final} changes when the electron density and atomic distances change, it can be used as a probe to study electron correlation. When U, or more specifically electron correlation dominates, the relaxation time increase.

XTDAS[34] can be used to detect and identify: 1. the progressive change in electron correlation as a function of temperature; 2. the detection of the appearance of electron density; and 3. the strength of vibration modes of specific bond. Figure 31 and 32 are plots of XTDAS vs. k space of $NiS_{1.48}Se_{0.62}$ at the Ni k Edge as a function of temperature. From Figure 31, the XTDAS slope increase with increasing temperature, which indicates the vibrational modes are different

with changes in temperature and the vibrational modes are stronger at higher temperature. Figure 32 indicates a change in EXAFS due to a decrease in electron density near the Ni atoms with increasing temperature. The XTDAS at the Se K Edge shown in Figure 34 indicates that the strongest vibrational modes are from the temperature range near or at the phase transition. These results suggest that, as $NiS_{1.48}Se_{0.62}$ undergoes a phase transition, the electron density around the Ni atoms decrease while the vibrational mode around the Se atoms increases, indicating that the material is becoming insulating and the AF ordering is more disordered than in the metallic phase.

Since there are no structural changes except in the vibrational mode of specific bonds, the sinusoidal oscillations in XTDAS are due to changes in the Debye-Waller factor (σ) and changes in the atomic distances and electron density around the absorber. As shown in Figure 33 and 35, σ for the Se-Ni and Ni-Se (just Ni-Se) bonds mirrors the changes in both EXAFS and XTDAS analysis. As the temperature is decreased from 70 K, σ is constant approaching the phase transition at about 25 K. Past the phase transition, σ becomes stable again.

Although the $NiS_{1.48}Se_{0.62}$ data has excellent signal to noise ratios (SNR) as shown in Figure 17, an interesting point to note when analyzing EXAFS data with poor SNR is the Fourier transformation. Conventional Fourier transformation techniques often have the disadvantage of distorting important spectral features and creating artifacts when SNR is low, resulting from increased noise in the data. There are two methods that take into account the properties of the Fourier transform such as the Hermite Expansion Method[35] (HEM) and the Maximum Entropy Method[36] (MEM) for noise filtering. A search for available filtering methods such as MEM and HEM to remove EXAFS noises in EXAFS $NiS_{1.48}Se_{0.62}$ without leaving artifacts was explored using EXAFSPAK, AutoSignal and maximum entropy method.

In discussion with Dr. Graham George, the creator of EXAFSPAK[31], via email and study of EXAFSPAK in detail, it was realized that EXAFSPAK does offer analysis toolkit such as maximum entropy along with fast Fourier and Simpson rule integration algorithm for data filtering. According to Dr. Graham George's suggestion, use of the maximum entropy method should be avoided since it is prone to artifacts. Attempts were made to use the maximum entropy option in EXAFSPAK, which resulted in the software crashing. This was primarily due to the instability of the software code to handle MEM's complex calculations. Both fast Fourier and Simpson rule method were also evaluated but did not show any improvements in achieving better SNR.

With the limitation of EXAFSPAK to effectively accomplish noise filtering, commercial software such as AutoSignal was explored as a tool for noise filtering. Dr. Joel Bondurant, a senior engineer/scientist for AutoSignal was contacted by email to determine if AutoSignal can filter noises in EXAFS. His response by email is as follows: "AutoSignal can remove noise using Fourier, Eigendecomposition, and Wavelet transforms. The only algorithm in AutoSignal based on Maximum Entropy methods is the Burg algorithm used to compute the AutoRegressive spectra. Since an AR smoothing procedure of inverses to the AR produces in AutoSignal, it will not be possible to remove noise based on Maximum Entropy using AutoSignal." He further informed us that he is not familiar with another product that performs MEM denoising."

Major drawbacks in using HEM and MEM in the analysis of $NiS_{1.48}Se_{0.62}$ are the availability of software to run HEM and MEM and integrating that software with EXAFSPAK.

5. CONCLUSIONS

EXAFS and XTDAS analysis of the XAS measurement of Abs. vs. T at Ni and Se k Edges for $NiS_{1.48}Se_{0.62}$ show excellent correlation with the phase diagram for an AF metal to WF insulator phase transition at 18 K. EXAFS analysis indicates that the relaxation time increases with increasing absorption post the Edge region are due to phase transition from AF to WF magnetic ordering. The changes measure in the EXAFS analysis is confirmed by XTDAS of strong vibrational modes occurring at the phase transition.

REFERENCES

1. Wilson, A. H. (1931a) Proc. R. Soc. Lond., A133, 458.

2. Wilson, A. H. (1931b) Proc. R. Soc. Lond., A134, 277.

3. Mott, N. F. (1956) Proc. Phys. Soc., A62, 416.

4. Hubbard, J. (1964a) Proc. R. Soc. London, 277, 237.

5. Sawatzky, G.A. (1987) Narrow-Band Phenomena-Influence of Electrons with Both Band and Localized Character, Plenum Press, New York and London.

6. Fujimori, A., Mirani, F. (1984) Phys. Rev. Lett., 53, 957.

7. Zaanen, J., Sawatzky, G.A., Allen, J.W. (1985) Phys. Rev. Lett., 55, 418.

8. Bither, T. A., Bouchard, R. J., Cloud, W. H., Donohue, P. C., Siemons, W. J. (1968) Inorg. Chem., 7, 2208.

9. Bouchard, R. J. J. (1968) Cryst. Growth, 2, 40.

10. Bouchard, R. J., Gillson, J. L., Jarrett, H. S. (1973) Mater. Res. Bull., 8, 489.

11. Jarrett, H. S., Bouchard, R. J., Gillson, J. L., Jones, G. A., Marcus, S. M., Weiher, J. F. (1973) Mater. Res. Bull., 8, 877.

12. Krill, G., Lapierre, M. F., Gautier, F., Robert, C., Czjzek, G., Fink, J., Schmidt, H. S. (1976) Phys. Chem. Solid State Phys., 9, 761.

13. Mabatah, N., Takahashi, H. (1980) J. Magn. Magn. Mater., 31, 335.

14. Kwizera, P., Dresselhaus, M. S., Adler, D. (1981) Phys. Rev., 21, 2328.

15. Matsuura, A. Y. (1997): 1997 SSRL Activity Report.

16. Honig, J. M. (1998) Chem. Mater., 10, 2910-2929.

17. Gautier, F. (1975) Phys. Lett., 53A, 31.

18. Thio, T., Bennett, J. W. (1995) PRB., 52, 3555.

19. Kronig, Z. (1932) Physik., 70, 317.

20. Mitchell, G., Beeman, W. W. (1952) J. Chem. Phys., 20, 1298.

21. Van Nordstrand, R. A. (1960) Advances in Catalysis, 12, 149.

22. Lytle, F. W. (1965) Physics of Non-Crystalline Solids, J. A. Prins, Ed., North-Holland, Amsterdam, 12.

23. Lytle, F. W. (1966) Adv. X-ray Analysis, 9, 398.

24. Levy, J. (1965) J. Chem. Phys., 43, 1846.

25. Sayers, D. E., Sten, E. A., Lytle, F. W. (1971) Phys. Rev. Lett., 27, 1204.

26. Sayers, D. E., Lytle, F. W., Sten, E. A. (1970) Adv. X-ray Anal., 13, 248.

27. Fricke, H. (1920) Phys. Rev., 16, 202.

28. Hertz, G., Zeit, F. (1920) Pysik., 3, 19.

29. Lytle, F. W., Sayers, D. E., Sten, E. A. (1975) Phys. Rev., B11, 4825.

30. Bither, T. A., Bouchard, R. J., Cloud, W. H., Donohue, P. C., Siemons, W. J. (1968) J. Inorg. Chem., 7, 2208.

31. George, M., Pickering, I. J. (1993) EXAFSPAK, SSRL Workshop.

32. Norman, T. (1999) Thesis: A X-ray Absorption Study of the MIT for $NiS_{1.52}Se_{0.48}$ sample.

33. Xiaoqiang, Y., Honig, J. M. (1994) Mater. Res. Bull., 29, 709.

34. Acrivos, J. (2002) J. Microchem., 71, 117.

35. Krylov, A. (2000) Phys. Chem. Chem. Phys., 2, 5743.

36. Matsubayashi, N. (1993) *Jpn. J. Appl. Phys.*, 32, 122.

TABLES

Table 1 XAS Data Files with Date and Time for $NiS_{2-x}Se_x$ (X=0.62) Data Acquisition at Ni K Edge

File	Date	Time
Ni-K-42-01	2/6/2000	12:09 PM
Ni-K-42-02	2/6/2000	12:26 PM
Ni-K-42-03	2/6/2000	12:43PM
Ni-K-42-04	2/6/2000	1:00 PM
Ni-K-42-05	2/6/2000	1:17 PM
Ni-K-42-06	2/6/2000	1:35 PM
Ni-K-42-07	2/6/2000	1:52 PM
Ni-K-42-55	2/7/2000	3:35 AM
Ni-K-42-08	2/6/2000	2:09 PM
Ni-K-42-09	2/6/2000	2:26 PM
Ni-K-42-10	2/6/2000	2:43 PM
Ni-K-42-11	2/6/2000	3:00 PM
Ni-K-42-12	2/6/2000	3:18 PM
Ni-K-42-13	2/6/2000	3:35 PM
Ni-K-42-14	2/6/2000	3:52 PM
Ni-K-42-15	2/6/2000	4:09 PM
Ni-K-42-16	2/6/2000	4:26 PM
Ni-K-42-17	2/6/2000	4:43 PM
Ni-K-42-18	2/6/2000	5:00 PM
Ni-K-42-19	2/6/2000	5:18 PM
Ni-K-42-20	2/6/2000	5:35 PM
Ni-K-42-22	2/6/2000	6:09 PM
Ni-K-42-23	2/6/2000	6:26 PM
Ni-K-42-24	2/6/2000	6:43 PM
Ni-K-42-25	2/6/2000	7:00 PM
Ni-K-42-26	2/6/2000	7:18 PM
Ni-K-42-27	2/6/2000	7:35 PM
Ni-K-42-28	2/6/2000	7:52 PM
Ni-K-42-29	2/6/2000	8:09 PM
Ni-K-42-30	2/6/2000	8:26 PM
Ni-K-42-31	2/6/2000	8:43 PM
Ni-K-42-32	2/6/2000	9:01 PM
Ni-K-42-33	2/6/2000	9:18 PM
Ni-K-42-34	2/6/2000	9:35 PM
Ni-K-42-35	2/6/2000	9:52 PM
Ni-K-42-36	2/6/2000	10:09 PM
Ni-K-42-37	2/6/2000	10:26 PM
Ni-K-42-38	2/6/2000	10:43 PM
Ni-K-42-39	2/6/2000	11:01 PM
Ni-K-42-40	2/6/2000	11:18 PM
Ni-K-42-41	2/6/2000	11:35 PM
Ni-K-42-42	2/6/2000	11:52 PM
Ni-K-42-43	2/7/2000	12:09 AM
Ni-K-42-44	2/7/2000	12:26 AM
Ni-K-42-45	2/7/2000	12:44 AM
Ni-K-42-46	2/7/2000	1:01 AM
Ni-K-42-47	2/7/2000	1:18 AM
Ni-K-42-48	2/7/2000	1:35 AM
Ni-K-42-49	2/7/2000	1:52 AM
Ni-K-42-50	2/7/2000	2:09 AM
Ni-K-42-51	2/7/2000	2:26 AM
Ni-K-42-52	2/7/2000	2:44 AM
Ni-K-42-53	2/7/2000	3:01 AM
Ni-K-42-54	2/7/2000	3:18 AM
Ni-K-42-56	2/7/2000	3:35 AM

Table 2 XAS Data Files with Date and Time for $NiS_{2-x}Se_x$ (X=0.62) Data Acquisition at Se K Edge

File	Date	Time
Se-K-28-01	2/3/2000	8:16 PM
Se-K-28-02	2/3/2004	8:57 PM
Se-K-28-03	2/3/2004	9:39 PM
Se-K-28-04	2/3/2004	10:20 PM
Se-K-28-05	2/3/2004	11:02 PM
Se-K-28-06	2/3/2004	11:44 PM
Se-K-28-07	2/4/2000	12:45 AM
Se-K-28-08	2/4/2000	1:07 AM
Se-K-28-09	2/4/2000	1:48 AM
Se-K-28-10	2/4/2000	2:30 AM
Se-K-28-11	2/4/2000	3:12 AM
Se-K-28-12	2/4/2000	3:53 AM
Se-K-28-13	2/4/2000	4:35 AM
Se-K-28-14	2/4/2000	5:16 AM
Se-K-28-15	2/4/2000	5:58 AM
Se-K-28-16	2/4/2000	6:40 AM
Se-K-28-17	2/4/2000	8:38 AM
Se-K-28-18	2/4/2000	9:19 AM
Se-K-28-19	2/4/2000	10:01 AM
Se-K-30-01	2/4/2000	5:08 PM
Se-K-30-02	2/4/2000	5:49 PM
Se-K-30-03	2/4/2000	6:31 PM
Se-K-30-04	2/4/2000	7:13 PM
Se-K-30-05	2/4/2000	7:54 PM
Se-K-30-06	2/4/2000	8:36 PM
Se-K-30-07	2/4/2000	9:17 PM
Se-K-30-08	2/4/2000	9:59 PM
Se-K-30-09	2/4/2000	10:41 PM
Se-K-30-10	2/4/2000	11:22 PM
Se-K-30-11	2/4/2000	12:04 AM
Se-K-30-12	2/4/2000	12:45 AM
Se-K-30-13	2/5/2000	1:27 AM
Se-K-30-14	2/5/2000	2:09 AM
Se-K-30-20	2/5/2000	2:50 AM
Se-K-30-15	2/5/2000	3:32 AM
Se-K-30-17	2/5/2000	4:13 AM
Se-K-30-18	2/5/2000	4:55 AM
Se-K-30-19	2/5/2000	5:37 AM
Se-K-30-16	2/5/2000	6:18 AM

Table 3 Temperature Collection as a Function of Time and Date for Se K Edge
Data Collection without conversion

Time, s,	ITC502.default.T1 K	6:34 PM Time	18:34 0:01	3-Feb-00
0.25	0.17	0:01		3-Feb-00
90.05	4.40	18:35	Se-K-27-32	3-Feb-00
150.05	4.50	18:36		3-Feb-00
210.06	4.60	18:37		3-Feb-00
270.07	4.30	18:38		3-Feb-00
330.07	4.30	18:39		3-Feb-00
390.07	4.40	18:40		3-Feb-00
450.08	5.60	18:41		3-Feb-00
510.09	4.80	18:42		3-Feb-00
570.09	4.50	18:43		3-Feb-00
630.09	5.00	18:44		3-Feb-00
690.10	5.00	18:45		3-Feb-00
750.11	5.00	18:46		3-Feb-00
810.11	6.00	18:47		3-Feb-00
870.12	6.10	18:48		3-Feb-00
930.12	6.10	18:49		3-Feb-00
990.12	6.40	18:50		3-Feb-00
1050.13	6.30	18:51		3-Feb-00
1110.14	6.50	18:52		3-Feb-00
1170.14	6.60	18:53		3-Feb-00
1230.14	6.60	18:54		3-Feb-00
1290.15	6.60	18:55		3-Feb-00
1350.16	6.70	18:56		3-Feb-00
1410.16	6.70	18:57		3-Feb-00
1470.16	6.60	18:58		3-Feb-00
1530.16	6.60	18:59		3-Feb-00
1590.18	6.70	19:00		3-Feb-00
1650.18	6.60	19:01		3-Feb-00
1710.25	6.70	19:02		3-Feb-00
1770.18	6.70	19:03		3-Feb-00
1830.20	6.60	19:04		3-Feb-00
1890.20	6.50	19:05		3-Feb-00
1950.20	6.60	19:06		3-Feb-00
2010.20	6.40	19:07		3-Feb-00
2070.22	6.40	19:08		3-Feb-00
2130.22	6.30	19:09		3-Feb-00
2190.22	6.40	19:10		3-Feb-00

Table 4 Temperature Collection as a Function of Time and Date for Ni K Edge
Data Collection after conversion. Data less than 8% 1-sigma are used in the
analysis

File Run #	Ave Temp	Range (H-L)	Temp diff	1 Sigma ((H-L/2mean)*100)	
Ni-K-42-01	61.8	65.7 - 57.9	7.8	6.3	%
Ni-K-42-02	53.3	57.8 - 48.8	9.0	8.4	%
Ni-K-42-03	43.5	48.7 - 38.3	10.4	12.0	%
Ni-K-42-04	32.4	38.2 - 26.6	11.6	17.9	%
Ni-K-42-05	22.9	26.4 - 19.4	7.0	15.3	%
Ni-K-42-06	18.2	19.4 - 16.9	2.5	6.9	%
Ni-K-42-07	15.8	16.9 - 14.7	2.2	7.0	%
Ni-K-42-55	13.9	14.7 - 13.1	1.6	5.8	%
Ni-K-42-08	13.1	13.1 - 13.0	0.1	0.4	%
Ni-K-42-09	12.4	12.9 - 11.9	1.0	4.0	%
Ni-K-42-10	11.5	11.9 - 11.0	0.9	3.9	%
Ni-K-42-11	10.7	11.0 - 10.3	0.7	3.3	%
Ni-K-42-12	10.0	10.3 - 9.6	0.7	3.5	%
Ni-K-42-13	9.5	9.6 - 9.3	0.3	1.6	%
Ni-K-42-14	9.0	9.3 - 8.7	0.6	3.3	%
Ni-K-42-15	9.1	9.4 - 8.7	0.7	3.9	%
Ni-K-42-16	9.2	9.4 - 8.9	0.5	2.7	%
Ni-K-42-17	8.4	8.9 - 7.9	1.0	6.0	%
Ni-K-42-18	7.8	7.9 - 7.7	0.2	1.3	%
Ni-K-42-19	7.9	8.1 - 7.7	0.4	2.5	%
Ni-K-42-20	7.8	8.1 - 7.5	0.6	3.8	%
Ni-K-42-21	7.6	7.5 - 7.6	0.1	0.7	%
Ni-K-42-22	7.6	7.7 - 7.5	0.2	1.3	%
Ni-K-42-23	7.3	7.5 - 7.1	0.4	2.7	%
Ni-K-42-24	7.0	7.1 - 6.9	0.2	1.4	%
Ni-K-42-25	7.0	7.1 - 6.9	0.2	1.4	%
Ni-K-42-26	7.0	7.1 - 6.9	0.2	1.4	%
Ni-K-42-56	4.0	4.1 - 3.9	0.0	0.2	%
Ni-K-42-49	1.0	1.1 - 0.9	0.1	5.5	%

Table 5 Temperature Collection as a Function of Time and Date for Se K Edge Data Collection after conversion. Data less than 8% 1-sigma are used in the analysis

File Run #	Ave Temp	Range (H-L)	Temp diff	1 Sigma ((H-L/2mean)*100)	
Se-K-30-04	80.6	81.2 - 79.9	1.3	0.8	%
Se-K-30-03	78.2	82.0 - 74.3	7.7	4.9	%
Se-K-30-02	69.8	74.1 - 65.5	8.6	6.2	%
Se-K-30-05	68.1	78.3 - 57.8	20.5	15.1	%
Se-K-30-01	59.1	65.3 - 52.8	12.5	10.6	%
Se-K-30-06	49.6	57.4 - 41.7	15.7	15.8	%
Se-K-30-07	36.5	41.3 - 31.6	9.7	13.3	%
Se-K-30-08	29.7	31.5 - 27.8	3.7	6.2	%
Se-K-30-09	27.1	27.8 - 26.4	1.4	2.6	%
Se-K-30-10	25.9	26.3 - 25.4	0.9	1.7	%
Se-K-30-11	25.3	25.4 - 25.2	0.2	0.4	%
Se-K-30-12	25.2	25.3 - 25.1	0.2	0.4	%
Se-K-30-13	25.1	25.1 - 25.0	0.1	0.2	%
Se-K-30-14	24.9	25.0 - 24.8	0.2	0.4	%
Se-K-30-18	24.8	24.8 - 24.8	0.0	0.0	%
Se-K-28-17	20.0	20.0 - 19.9	0.1	0.3	%
Se-K-28-16	19.9	20.0 - 19.8	0.2	0.5	%
Se-K-28-15	19.7	19.8 - 19.6	0.2	0.5	%
Se-K-28-14	19.6	19.6 - 19.6	0.0	0.0	%
Se-K-28-19	19.5	19.5 - 19.5	0.0	0.0	%
Se-K-28-11	19.4	19.6 - 19.2	0.4	1.0	%
Se-K-28-10	19.2	19.2 - 19.1	0.1	0.3	%
Se-K-28-09	19.0	19.1 - 18.9	0.2	0.5	%
Se-K-28-08	18.8	18.9 - 18.7	0.2	0.5	%
Se-K-28-07	18.4	18.7 - 18.1	0.6	1.6	%
Se-K-28-06	18.0	18.1 - 17.8	0.3	0.8	%
Se-K-28-05	17.1	17.7 - 16.5	1.2	3.5	%
Se-K-28-04	15.6	16.4 - 14.7	1.7	5.5	%
Se-K-28-03	14.2	14.7 - 13.7	1.0	3.5	%
Se-K-28-02	14.1	14.5 - 13.6	0.9	3.2	%
Se-K-28-01	11.2	14.6 - 7.7	6.9	30.9	%
Se-K-27-32	6.1	7.7 - 4.4	3.3	27.3	%
Se-K-30-23	5.4	6.2 - 4.6	1.6	14.8	%
Se-K-30-22	5.3	5.9 - 4.7	1.2	11.3	%

Table 6 Determination of atomic position of $NiS_{2-x}Se_x$ for x =0.62

Look up Crystal structure positions PA3

Atomic Position for A compound in PA3			
Element	x	y	z
S4	0.1075	-0.3925	0.8925
S7	0.3925	0.1075	0.8925
Ni2	0.0000	0.5000	0.5000
Ni3	0.5000	0.0000	0.5000
S1	0.3925	0.3925	0.3925
S6	0.1075	0.8925	0.3925
S3	-0.3925	0.8925	0.1075
S8	0.8925	0.3925	0.1075
Ni1	0.0000	0.0000	0.0000
Ni4	0.5000	0.5000	0.0000
S2	0.8925	0.1075	-0.3925
S5	-0.3925	-0.3925	-0.3925
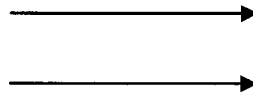
Multiply x,y,z by lattice parameter

Atomic Position for X=0.6, a=5.7705			
Element	x	y	z
site	0.0000	0.0000	0.0000
S4	0.6203	-2.2649	5.1502
S7	2.2584	0.6203	5.1502
Ni2	0.0000	2.8853	2.8853
Ni3	2.8853	0.0000	2.8853
S1	2.2584	2.2584	2.2584
S6	0.6203	5.1502	2.2584
S3	-2.2649	5.1502	0.6203
S8	5.1502	2.2584	0.6203
Ni1	0.0000	0.0000	0.0000
Ni4	2.8853	2.8853	0.0000
S2	5.1502	0.6203	-2.2649
S5	-2.2649	-2.2649	-2.2649

From Vegard's plot of $NiS_{2-x}Se_x$ for x=0.6, the lattice parameter is 5.7705 Angstrom

Since PA3 space group where a=b=c (cubic), x, y, and z is multiplied by the lattice parameter to give table shown above

D=Sqrt((xa-xb)^2+(ya-yb)^2+(za-zb)^2)

Element	Ni1 (000)	Ni2 (000)	Ni3 (000)	Ni4 (000)
	Atomic Distances between Ni and others, x=0.6			
S4	5.6603	5.6603	3.9230	7.6275
S7	5.6577	3.9192	2.4306	5.6610
Ni2	4.0804	0.0000		
Ni3	4.0804	4.0804	0.0000	
S1	3.9117	2.4262	2.4262	2.4262
S6	5.6577	2.4306	5.6610	3.9192
S3	5.6603	3.9230	7.6275	5.6603
S8	5.6577	5.6610	3.9192	2.4306
Ni1	0.0000			
Ni4	4.0804	4.0804	4.0804	0.0000
S2	5.6603	7.6275	5.6603	3.9230
S5	3.9230	7.6275	7.6275	7.6275

D=Sqrt((xa-xb)^2+(ya-yb)^2+(za-zb)^2)

Element	S1 (000)	S2 (000)	S3 (000)	S4 (000)	S5 (000)	S6 (000)	S7 (000)	S8 (000)
	Atomic Distances between S and others, x=0.6							
S4	5.6130	9.1557	9.1557	0.0000	7.9566	7.9590	3.3178	
S7	3.3235	7.9590	7.8422	3.3178	9.1525	5.6183	0.0000	5.6183
Ni2	2.4262	7.6275	3.9230	5.6603	7.6275	2.4306	3.9192	5.6610
Ni3	2.4262	5.6603	7.6275	3.9230	7.6275	5.6610	2.4306	3.9192
S1	0.0000	5.6130	5.6130	5.6130	7.8346	3.3235	3.3235	3.3235
S6	3.3235	7.8422	3.3178	7.9590	9.1525	0.0000	5.6183	5.6183
S3	5.6130	9.1557	0.0000	9.1557	7.9566	3.3178		7.9590
S8	3.3235	3.3178	7.9590	7.8422	9.1525	5.6183	5.6183	0.0000
Ni1	3.9117	5.6603	5.6603	5.6603	3.9230	5.6577	5.6577	5.6577
Ni4	2.4262	3.9230	5.6603	7.6275	7.6275	3.9192	5.6610	2.4306
S2	5.6130	0.0000	9.1557	9.1557	7.9566		7.9590	3.3178
S5	7.8346	7.9566	7.9566	7.9566	0.0000	9.1525	9.1525	9.1525

Wilson's rule[1] 1931: partially filled energy band → metal
otherwise → insulator
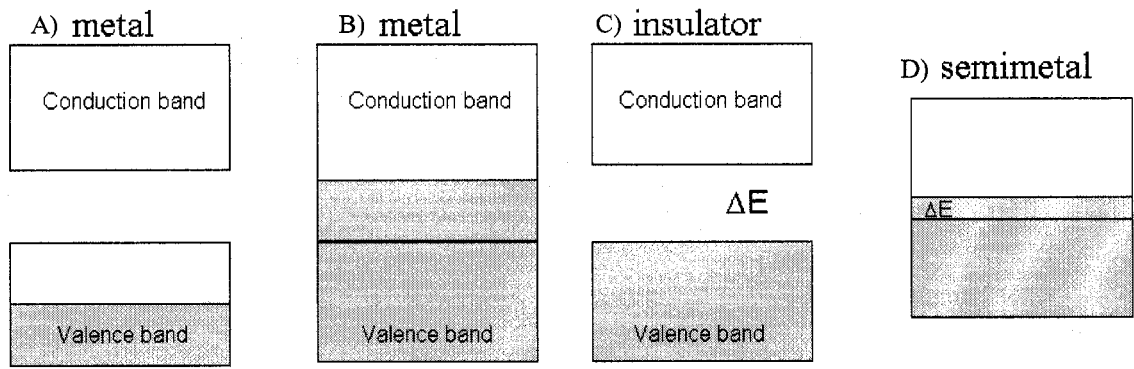
Figure 1. Wilson's band theory model for distinguishing between metal,
insulator, and semiconductors in solids. Metal can have partial fill valence band
(A) or overlapping valence and conduction bands (B). Insulator or semimetal
differs from metal by a characteristic energy gap (C) (D).

A) Ni   **B) Ni-X**   **C) Correlation**
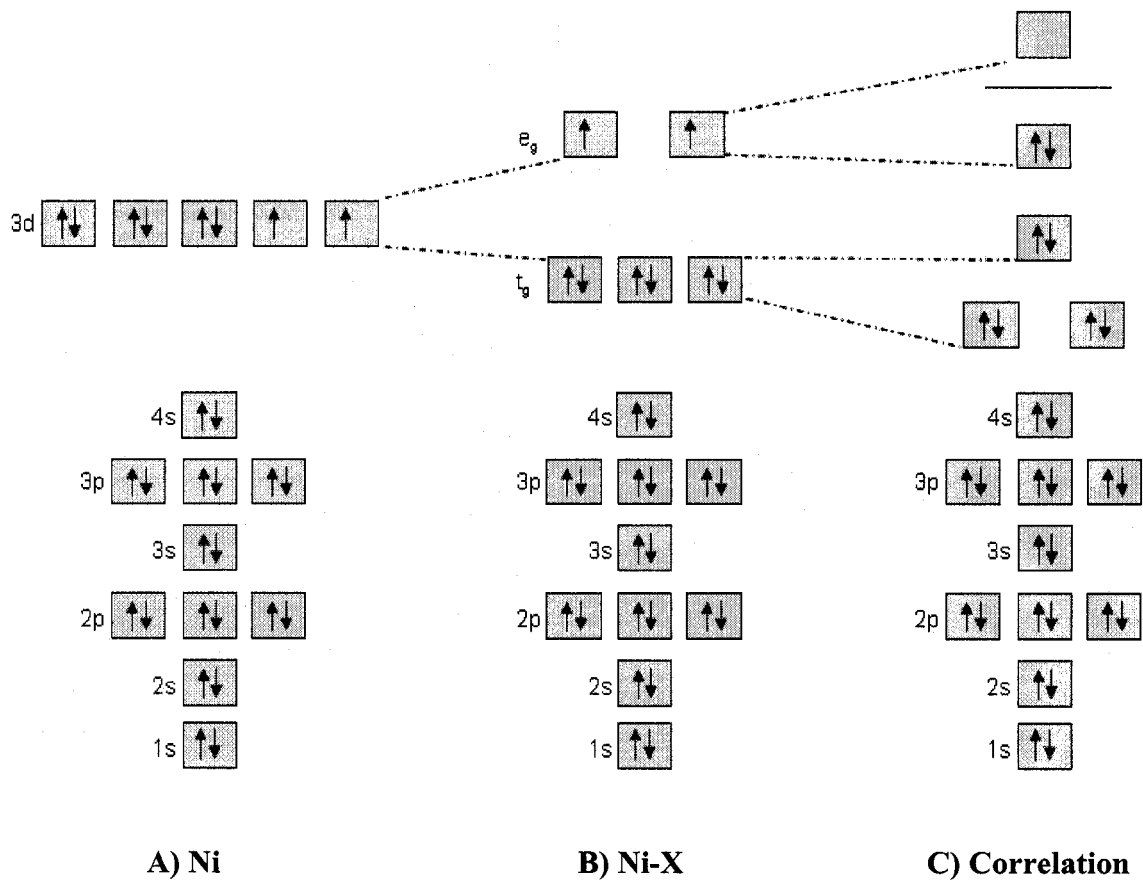
Figure 2. Electron configuration for Ni atom (A) and Ni cation (B) bonded to an anion (X) and effect of electron correlation (C). Crystal field will split the 3d states (A) into e_g and t_g symmetries (B). Since e_g level is partially filled, metallic properties are predicted as observed in $NiSe_2$. When there is strong electron correlation, e_g and t_g symmetries are further split as shown in (C). With no partial filled level and an energy gap, the material is insulating as observed in NiS_2.

41
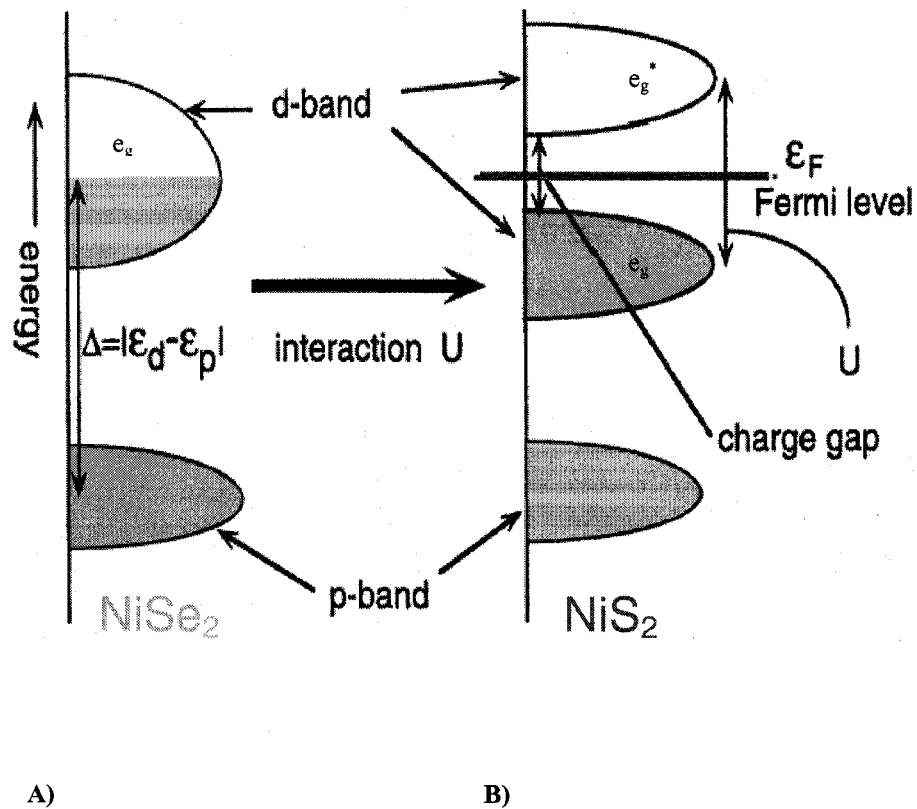
Figure 3. Electron orbital of the p and d states of $NiSe_2$ and NiS_2. In $NiSe_2$ (A), electron are partial filled in the e_g band; therefore, metallic properties are predicted. In NiS_2 (B), electron correlation breaks the e_g band resulting in an energy gap. Insulating properties are predicted.
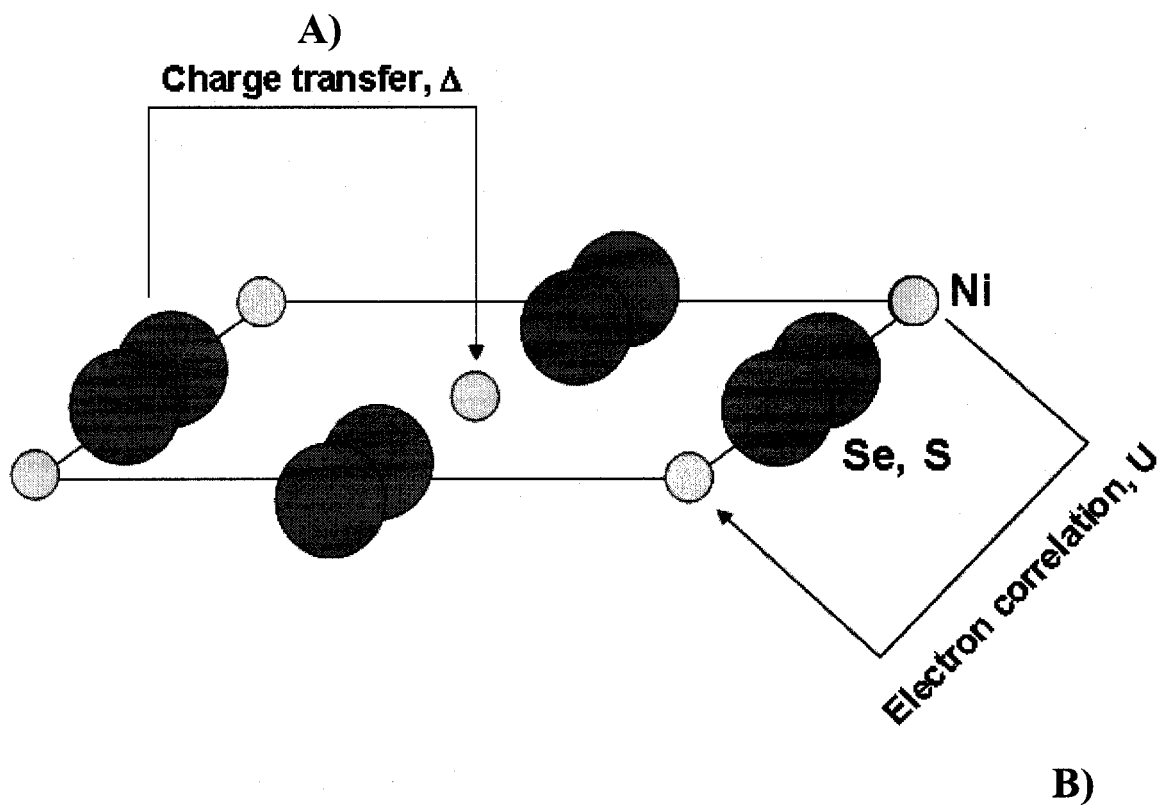
Figure 4. Representation of the ionic lattice consisting of either $NiSe_2$ or NiS_2. A) charge fluctuation due to charge transfer as a result of interaction between cation (Ni^{2+}) and anion (S^- or Se^-). B) charge fluctuation due to electron correlation as a result of cation to cation interaction
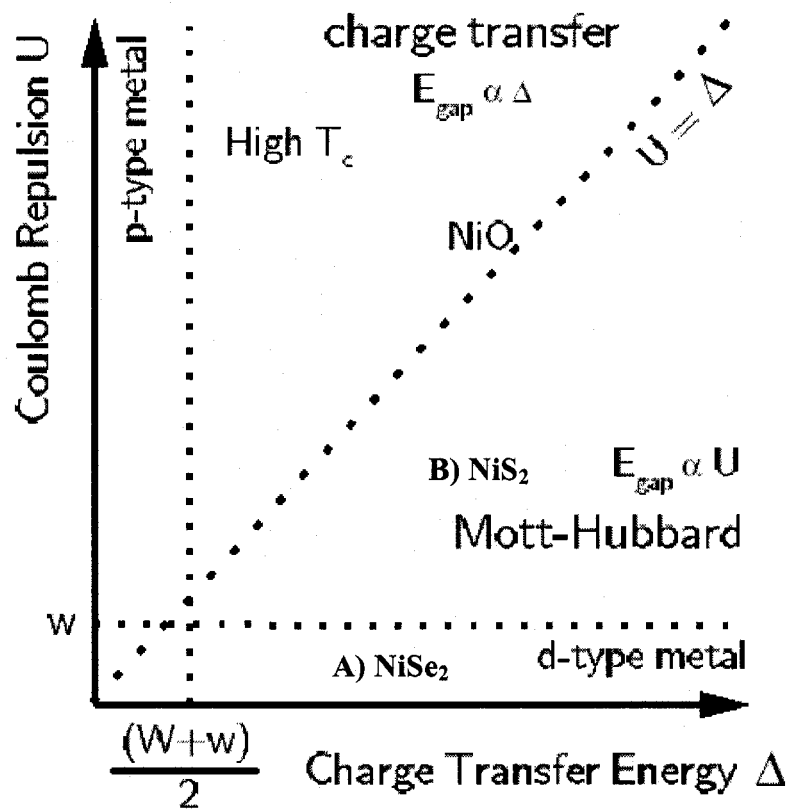
Figure 5. The various insulating and metallic conditions as found among the pyrite structures such as $NiSe_2$ and NiS_2 in the Zaanen-Sawatzky-Allen scheme as taken from reference 7. A) is where NiSe2 is placed when Δ dominates over U but less than W. B) is where NiS2 is placed when U dominates over U and W.
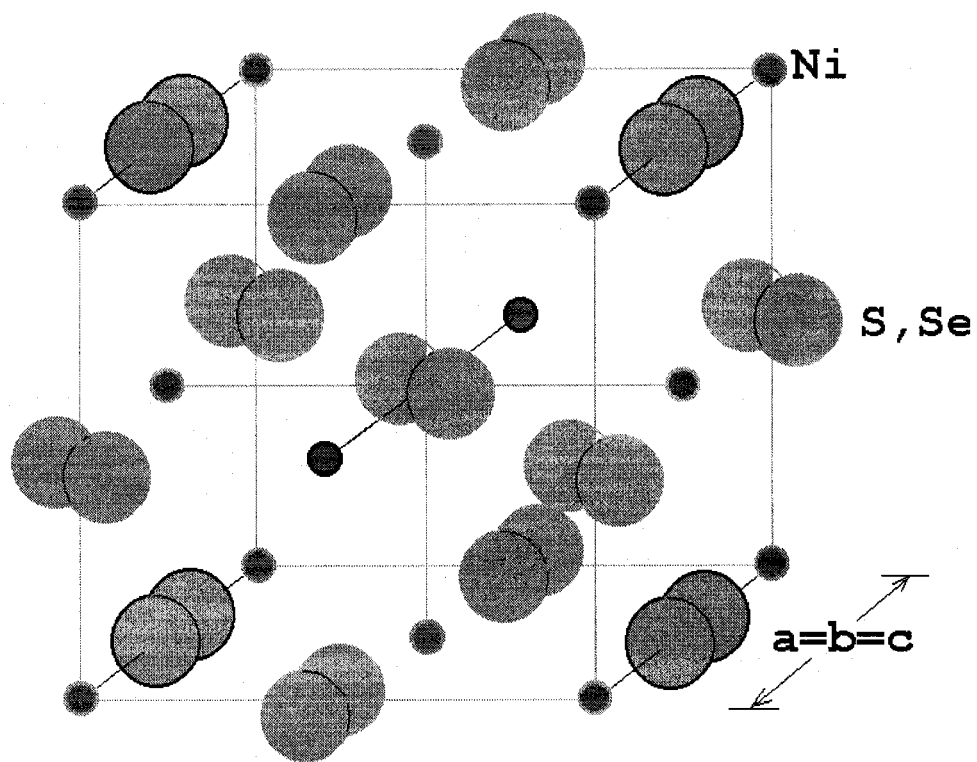
Figure 6. Pyrite Structure of $NiS_{2-x}Se_x$ with face-center cubic geometry and P3A space group. Ni^{2+} occupies octahedral symmetry and S/Se atoms occupying tetrahedral symmetry.
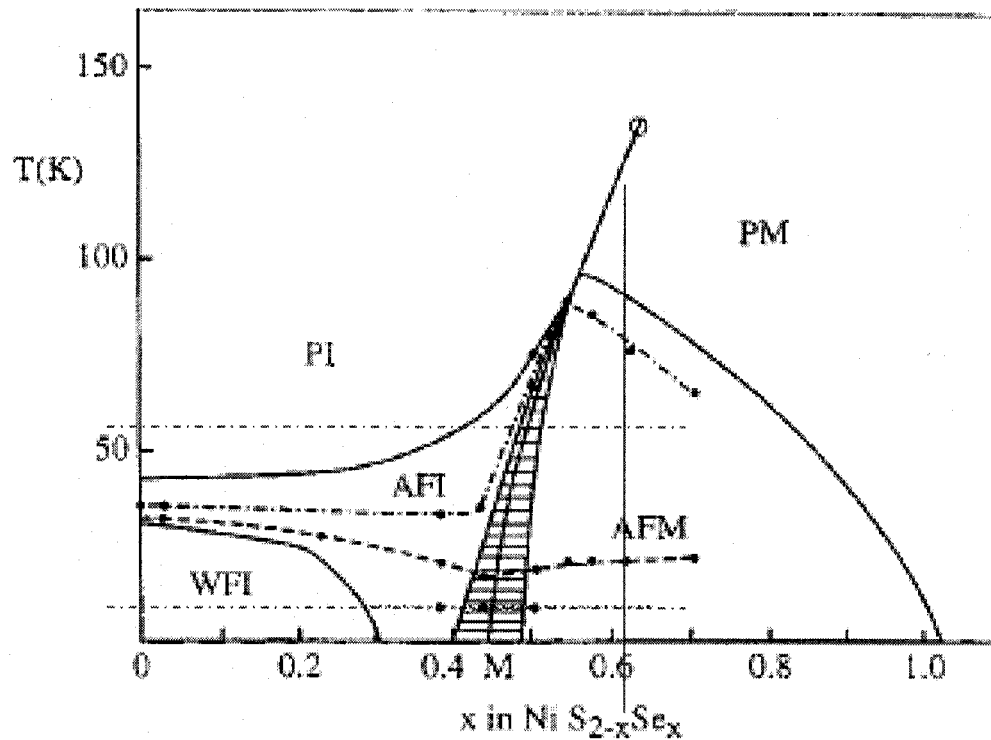
Figure 7. Phase diagram of $NiS_{2-x}Se_x$ system taken from reference 16. PI = paramagnetic insulator, PM = paramagnetic metal, WFI = weak ferromagnetic insulator, AFI = Anti-ferromagnetic insulator, AFM = anti-ferromagnetic metal. [taken from reference 16]
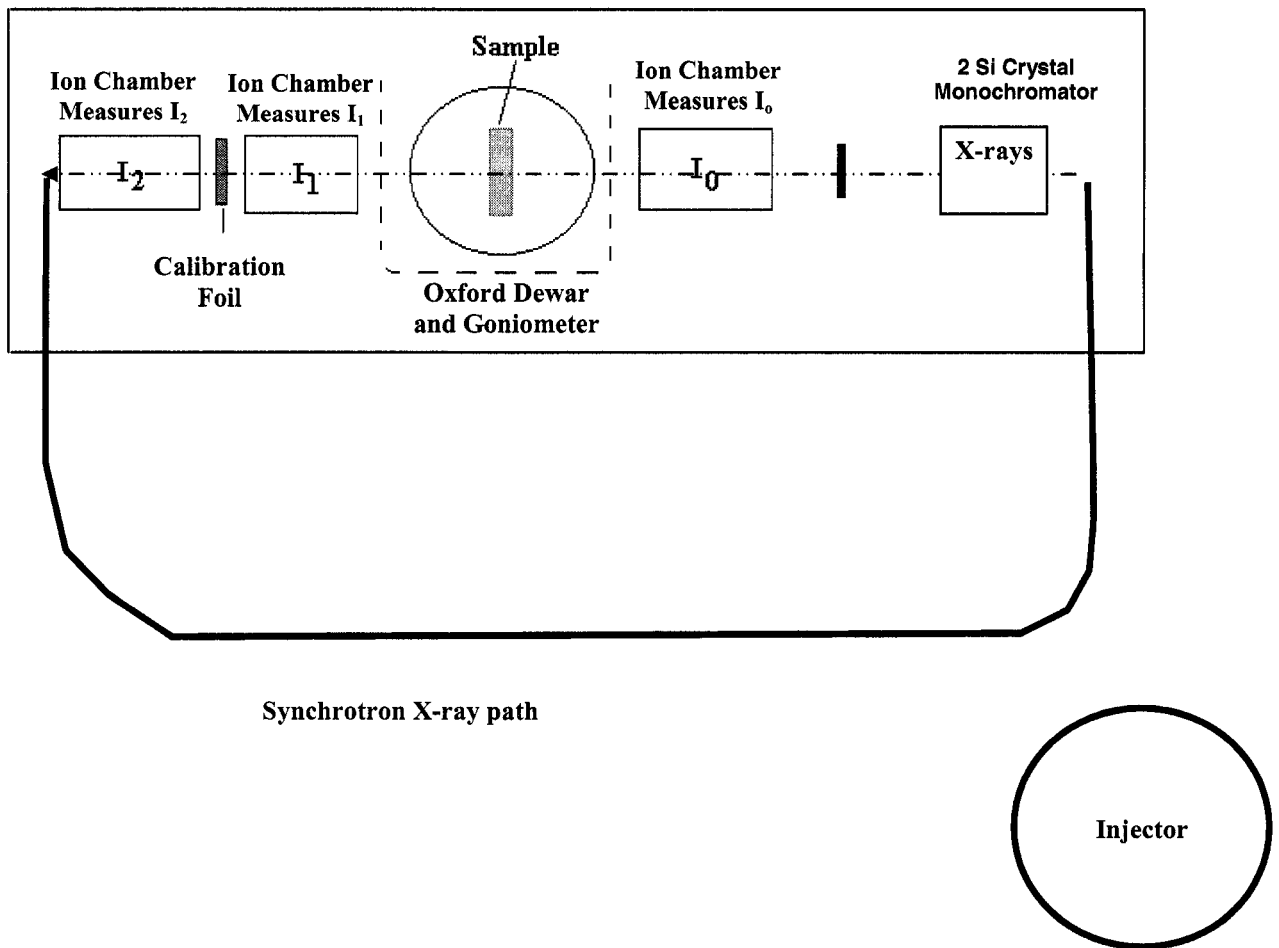
Figure 8. Layout of Synchrotron X-ray generated from the injector, fed into the Synchrotron X-ray path and through $NiS_{2-x}Se_x$ sample for data acquisition.

NiK Edge Temperature Range

Se-K Edge Temperature Range
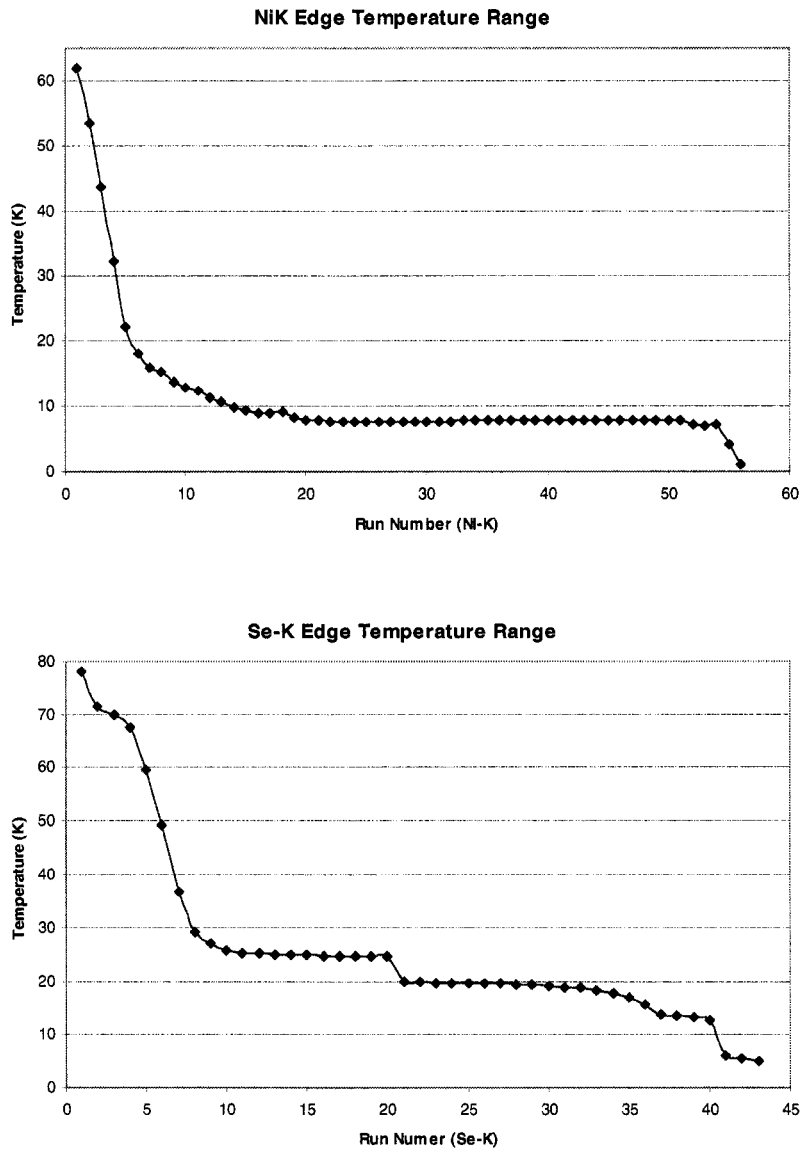
Figure 9. Temperature as a function of run number for XAS acquisition at Ni and Se K Edges. The temperature range from 70 to 0.5K was evaluated to only detect AF metal to WF insulator. A device is used to adjust a knob that controls the helium flow into the sample holder to control the temperature. The insensitivity of the device can cause temperature shifts such at run number 20 and 40
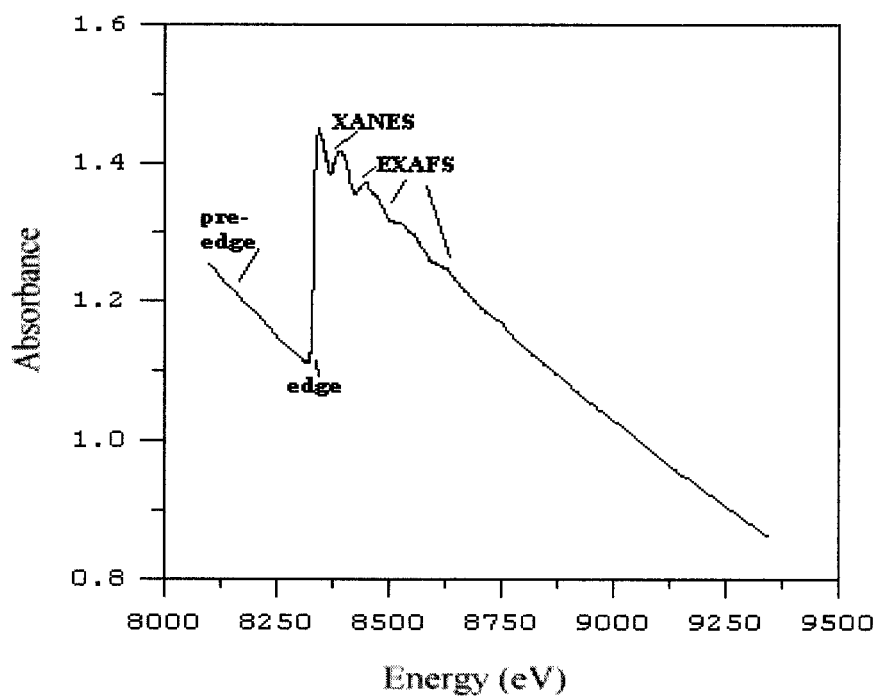
Figure 10. A typical XAS absorption spectrum as function of energy, which consists of four regions: Pre-Edge, Edge, XANES (X-ray Absorption Near Edge Structure), and EXAFS (Extended X-ray Absorption Fine Structure).
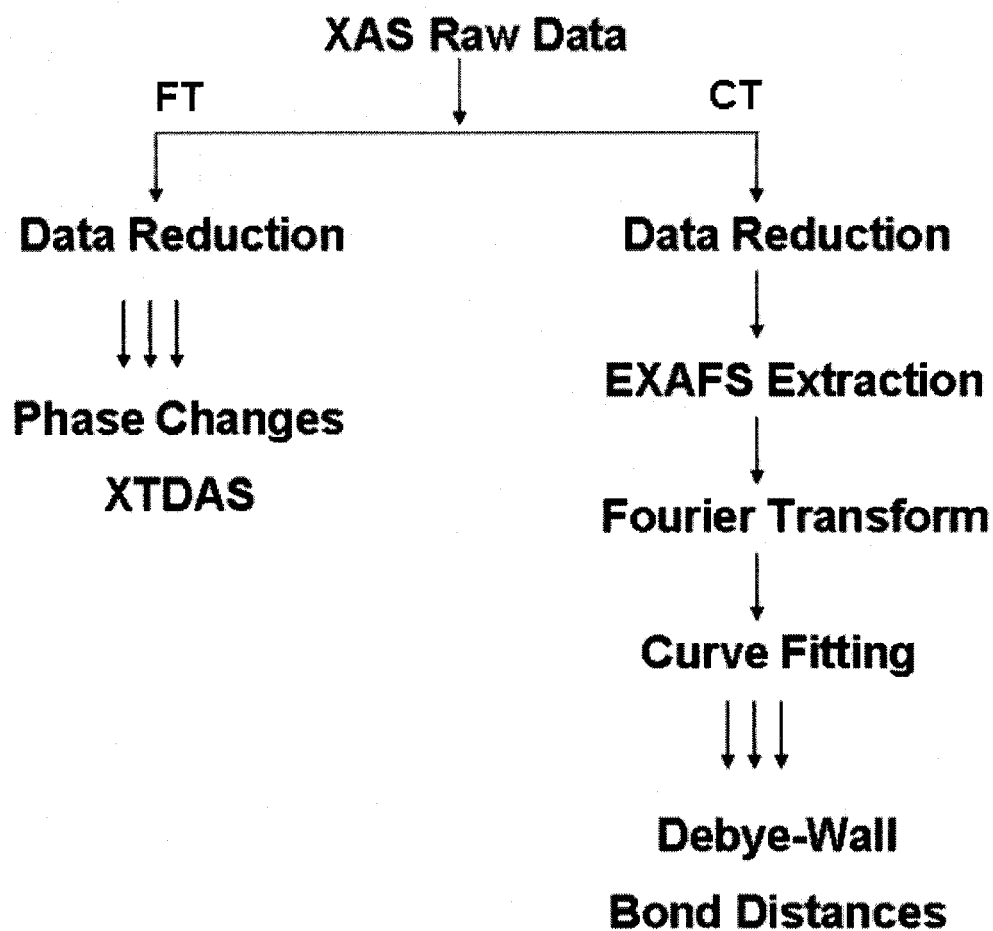
Figure 11. Approach for XAS analysis. Phase changes and XTDAS information is obtained from approach (FT). Debye-Wall and bond distances are obtained from approach (CT).
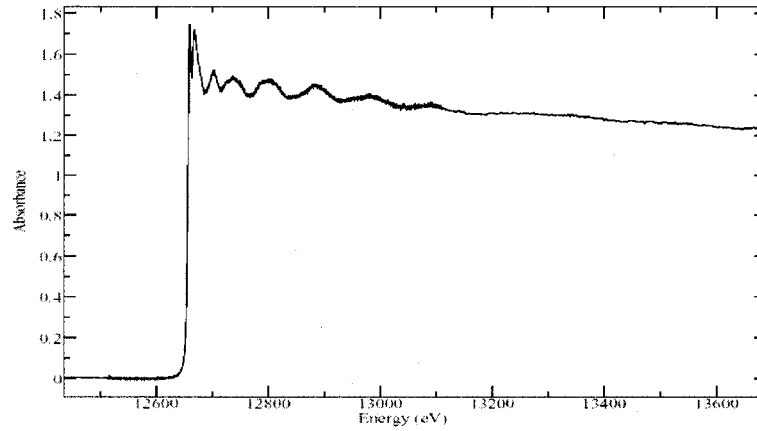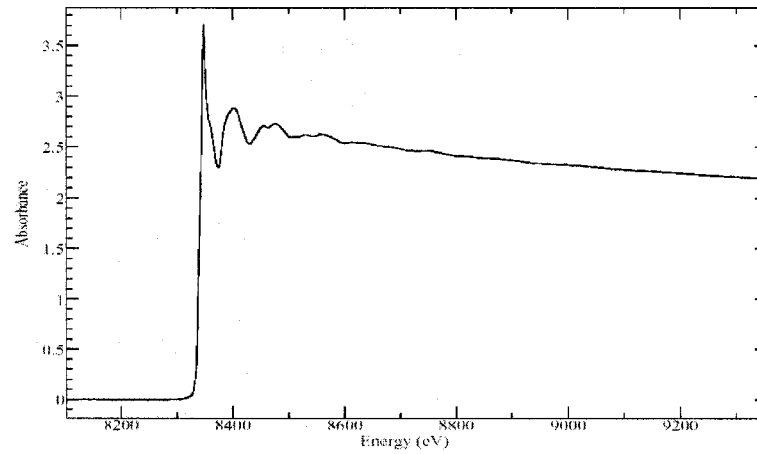
Figure 12. XAS (Absorbance) versus Energy at Ni and Se K Edges at T = 8K with EXAFS filtered from data reduction step in EXAFSPAK. Region of XAS absorption spectrum is described in Figure 10.
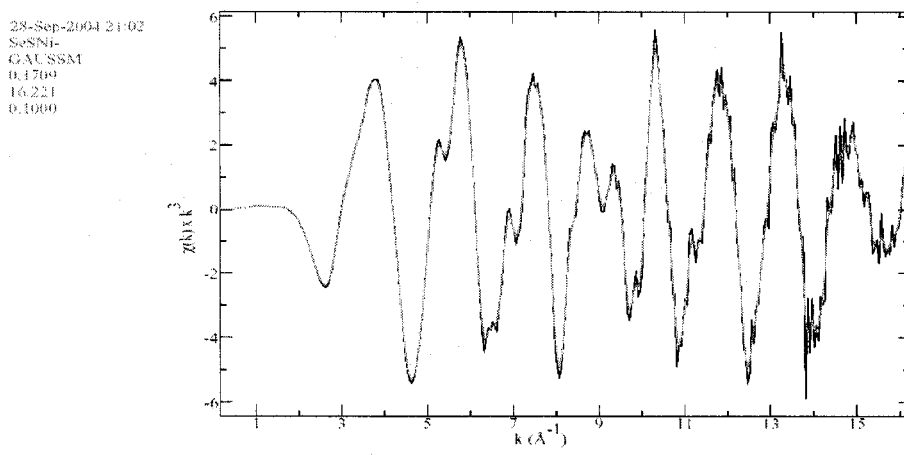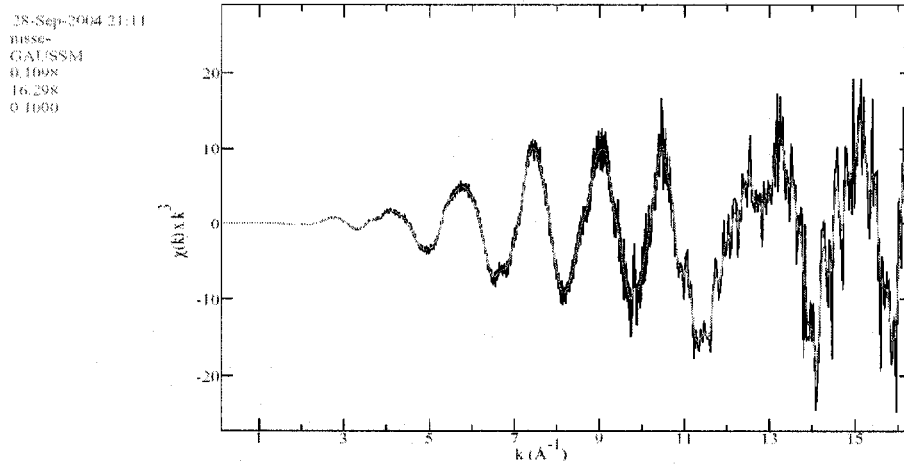
Figure 13. EXAFS region extracted from the filtered EXAFS data from Figure 11 for Ni and Se Edges at T = 8K. The modulation of the adsorption coefficient decays from right to left for the Se and Ni K Edge spectrums.
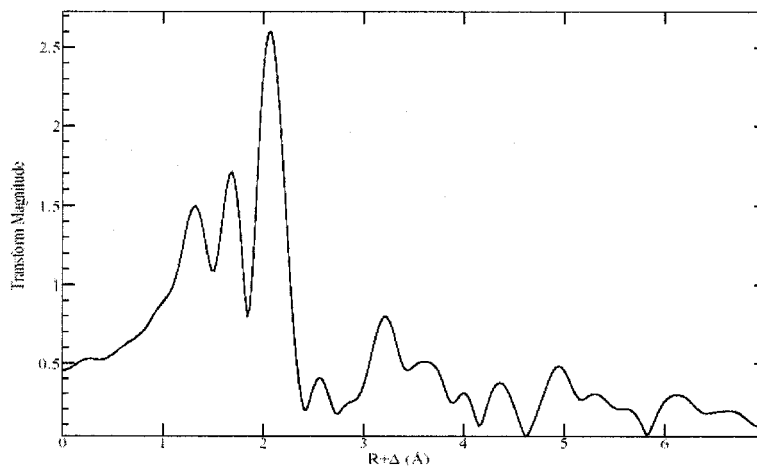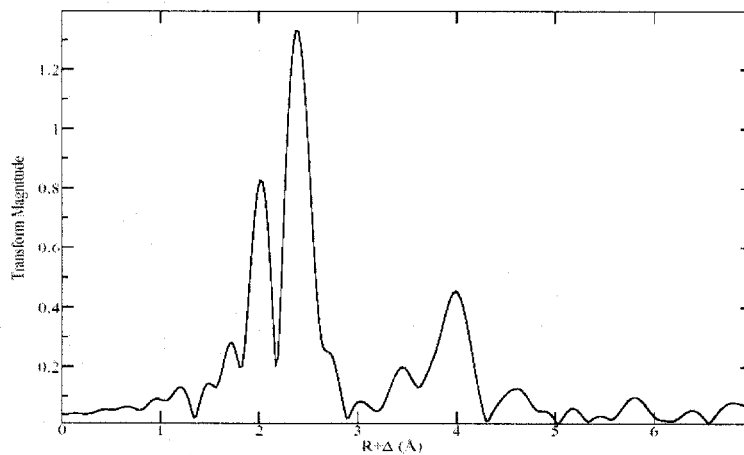
Figure 14. Exact Fourier transform of the filtered EXAFS in unit of $k3\chi(k)$ in momentum (k) distance space over the finite k range to distance r space for Ni and Se Edges at T = 8K. In theory each peak in FT-EXAFS spectrum corresponds to one coordination shell and the amplitude of the peak is dependent upon the number of atoms in that shell.
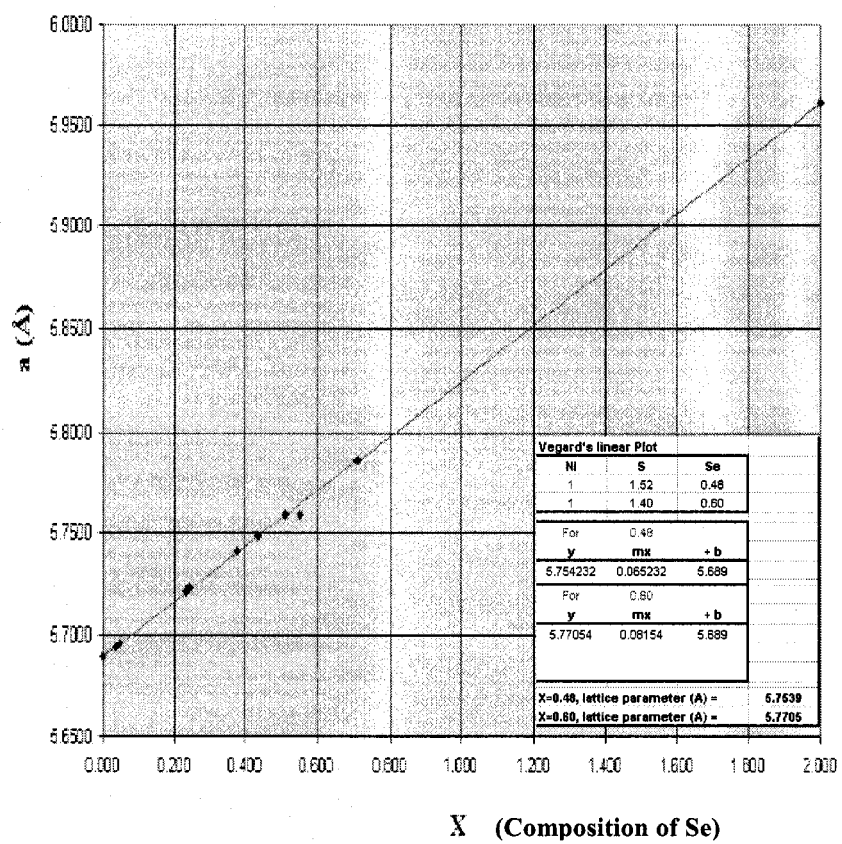
X (Composition of Se)

Figure 15. Vegard's Law plot of unit cell dimension as a function of composition for $NiS_{2-x}Se_x$ taken from reference 32
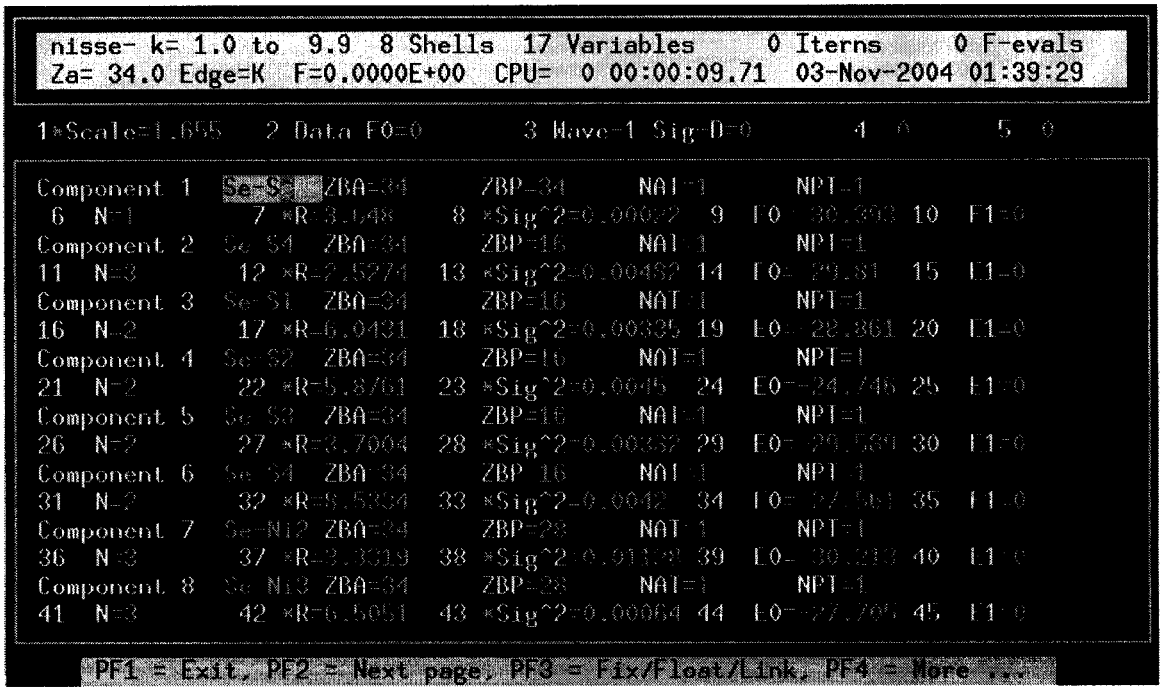
Figure 16. OPT-EXAFSPAK™ Marquardt Algorithm for Curve fitting $NiS_{2-x}Se_x$. The number of coordination (N), bond type, and bond distance of $NiS_{2-x}Se_x$ are entered into the software for curve fitting based on the generated $NiS_{2-x}Se_x$ model compound.
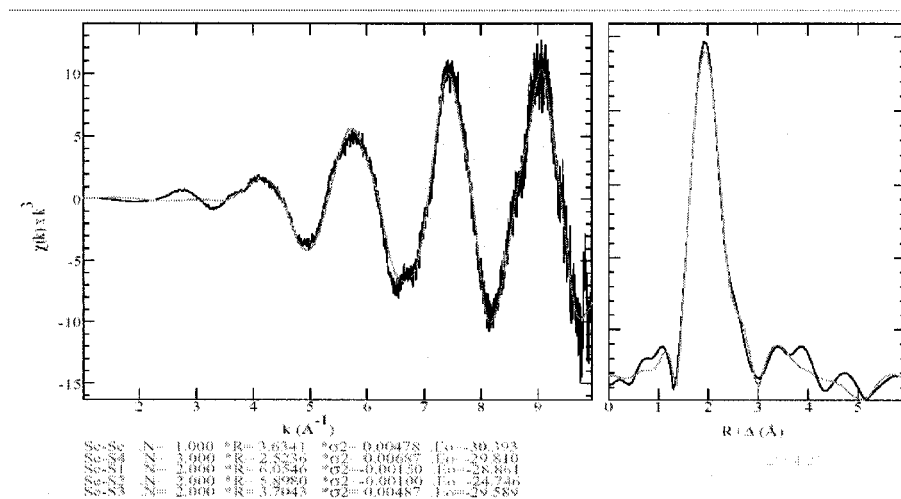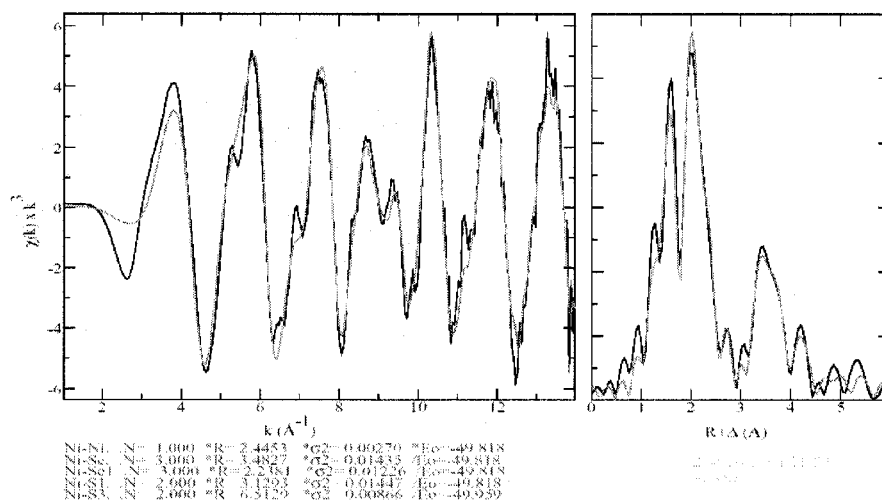
Figure 17. FT-EXAFS Curve Fit Result for Ni and Se Edges at T = 8K. Left spectrum is the curve fit to the EXAFS region. Right spectrum is the Fourier Transform of the EXAFS region.
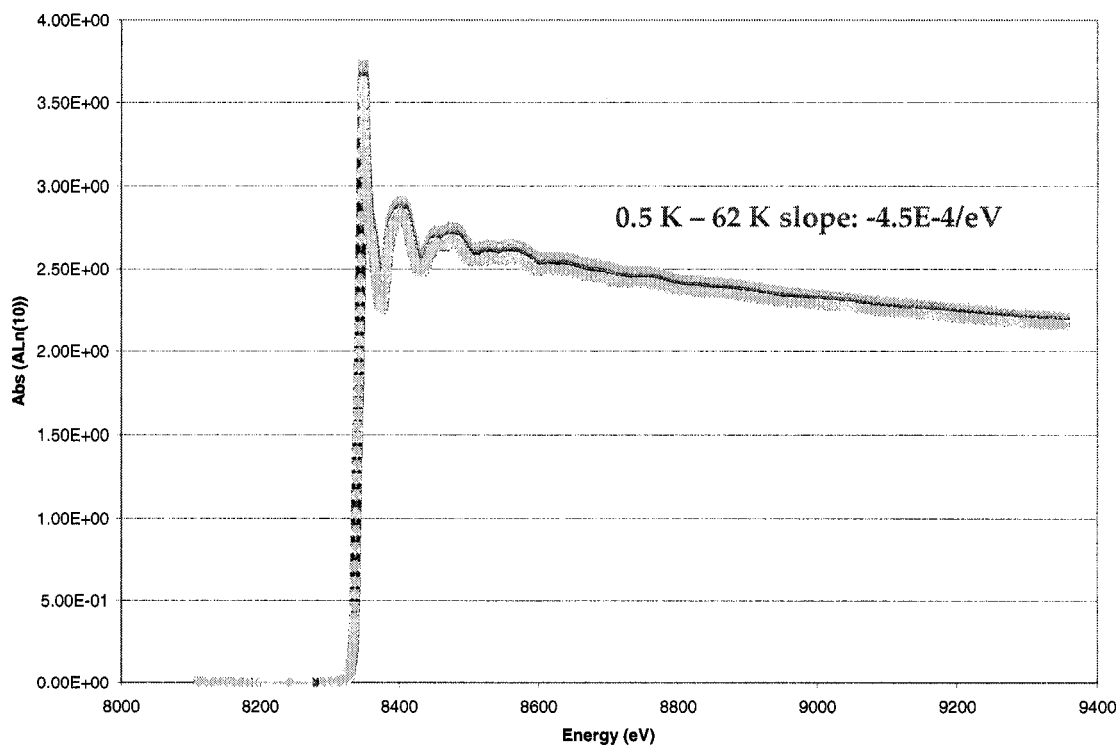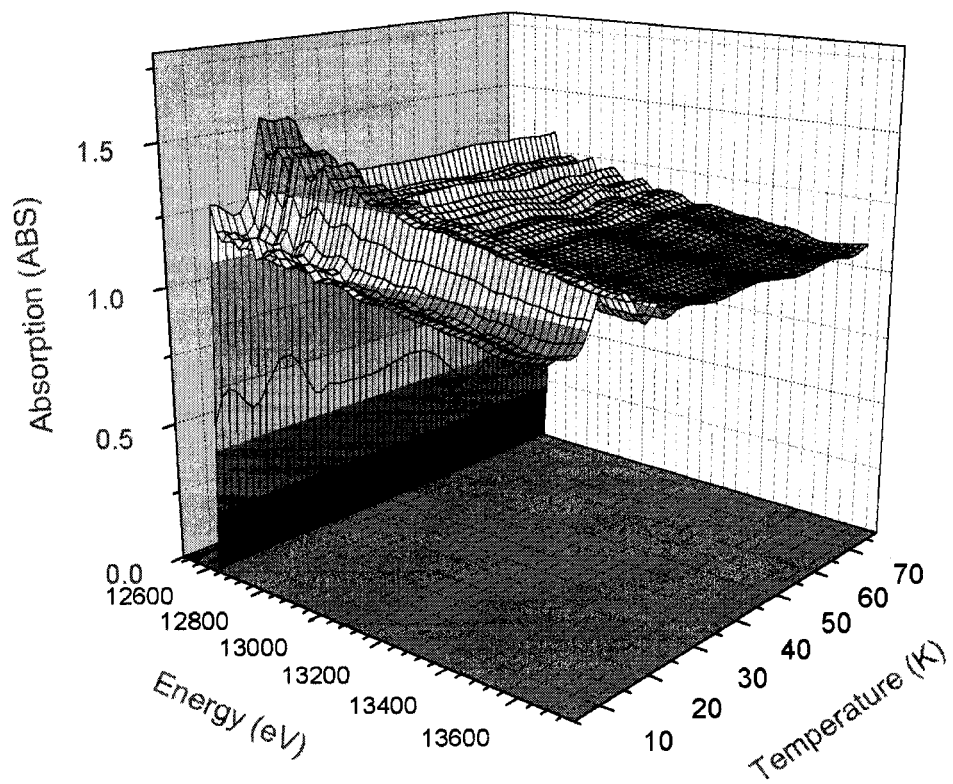
Figure 18. 2D plot of superimposed XAS spectrums at 0.5 K to 62 K of Ni at K Edge of data file shown in Table 1 after data reduction using EXAFSPAK™
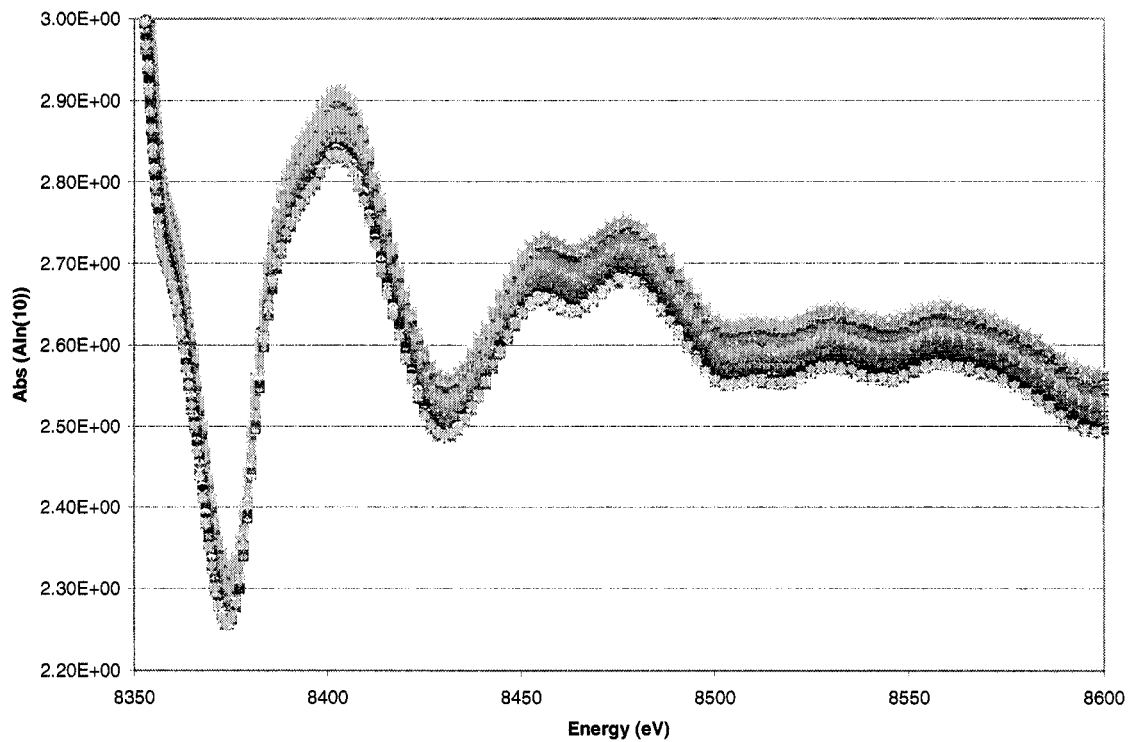
Figure 19. 2D plot of superimposed XAS spectrums magnified at EXAFS region of data file shown in Table 1 and Figure 18 after data reduction using EXAFSPAK™
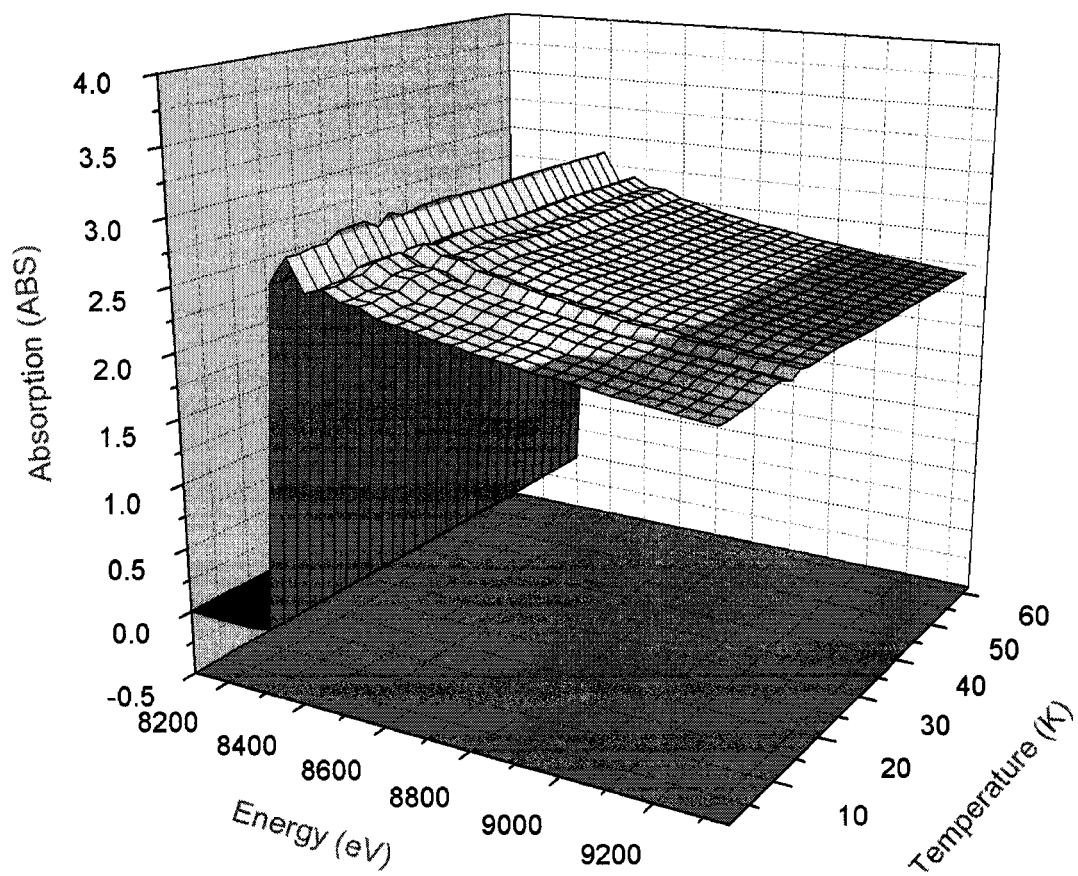
Figure 20. 3D plot of superimposed XAS spectrums at 0.5K to 62 K of Ni at K Edge of data file shown in Table 1 after data reduction using EXAFSPAK™
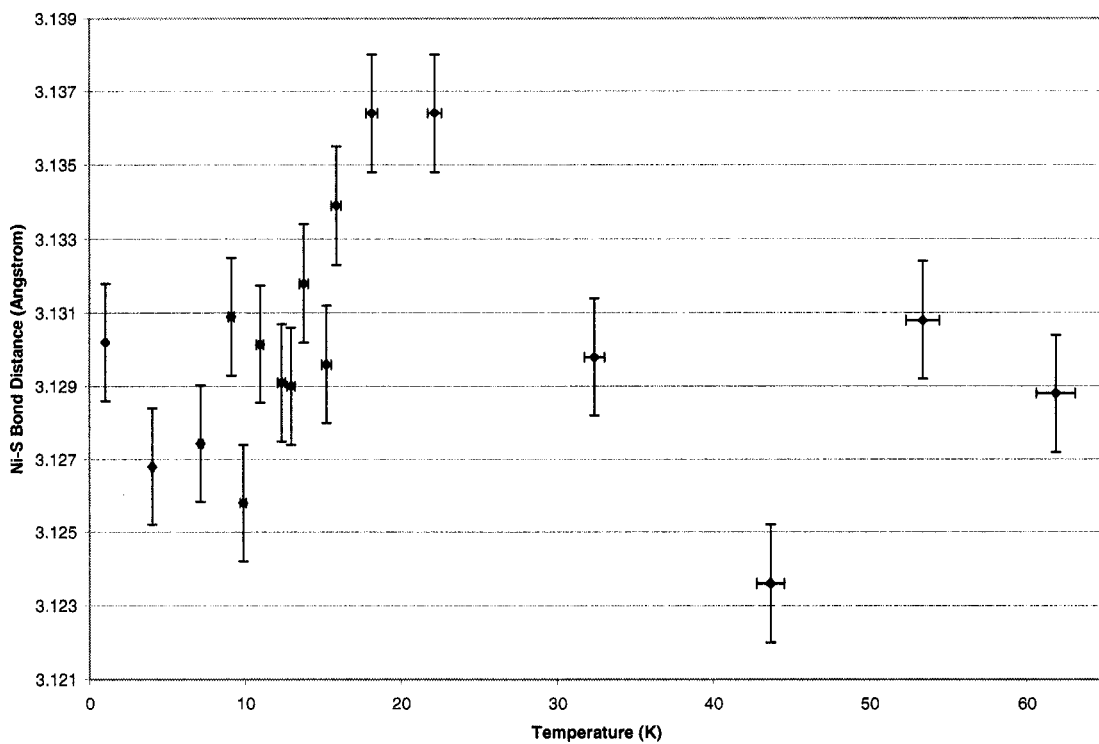
Figure 21. Ni-S bond distances versus temperature at Ni K Edge for $NiS_{1.38}Se_{0.62}$.
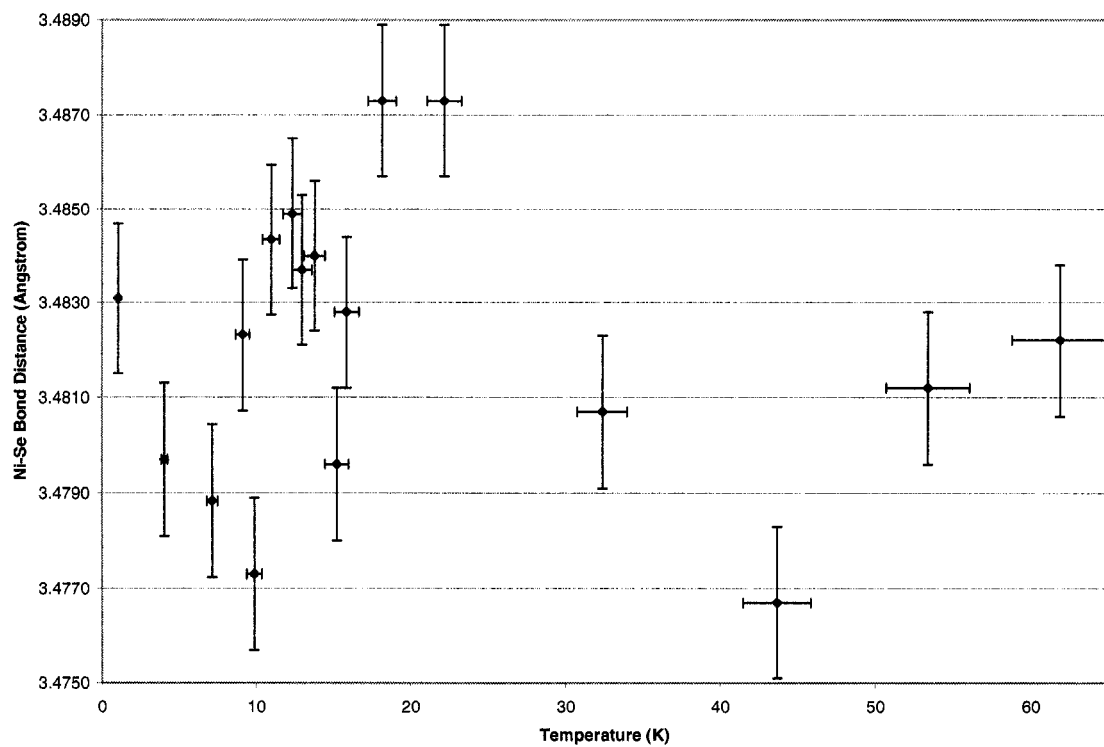
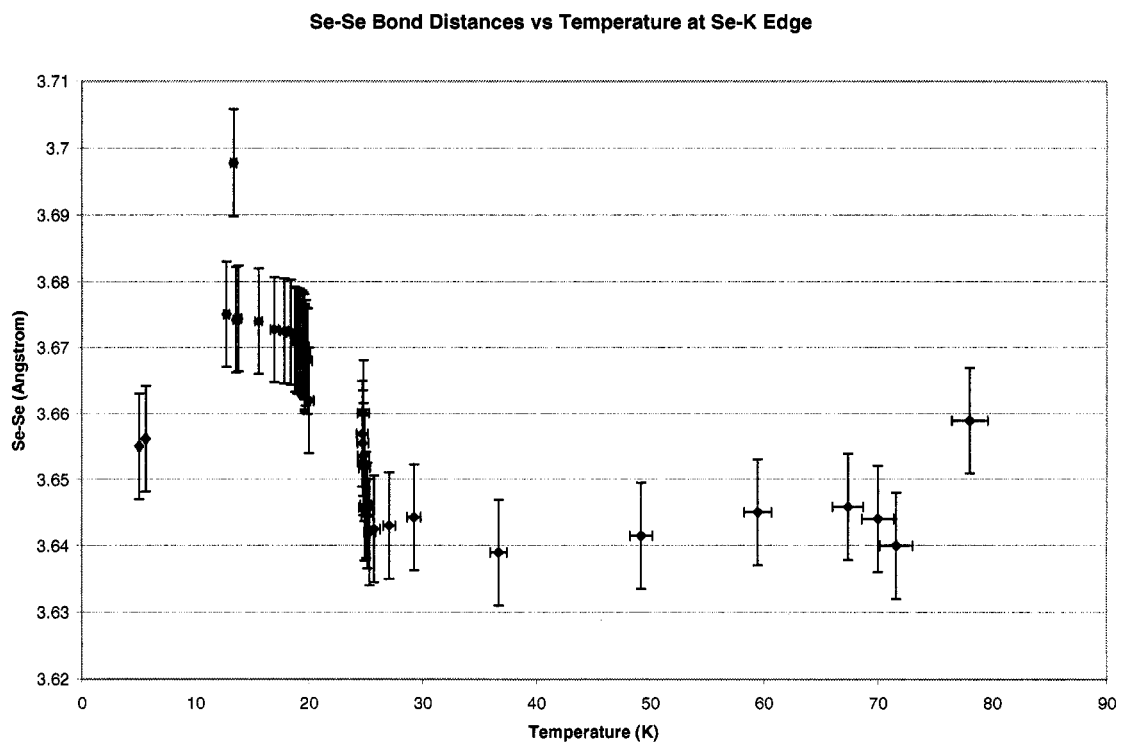Figure 22. Ni-Se bond distances versus temperature at Ni K Edge for $NiS_{1.38}Se_{0.62}$
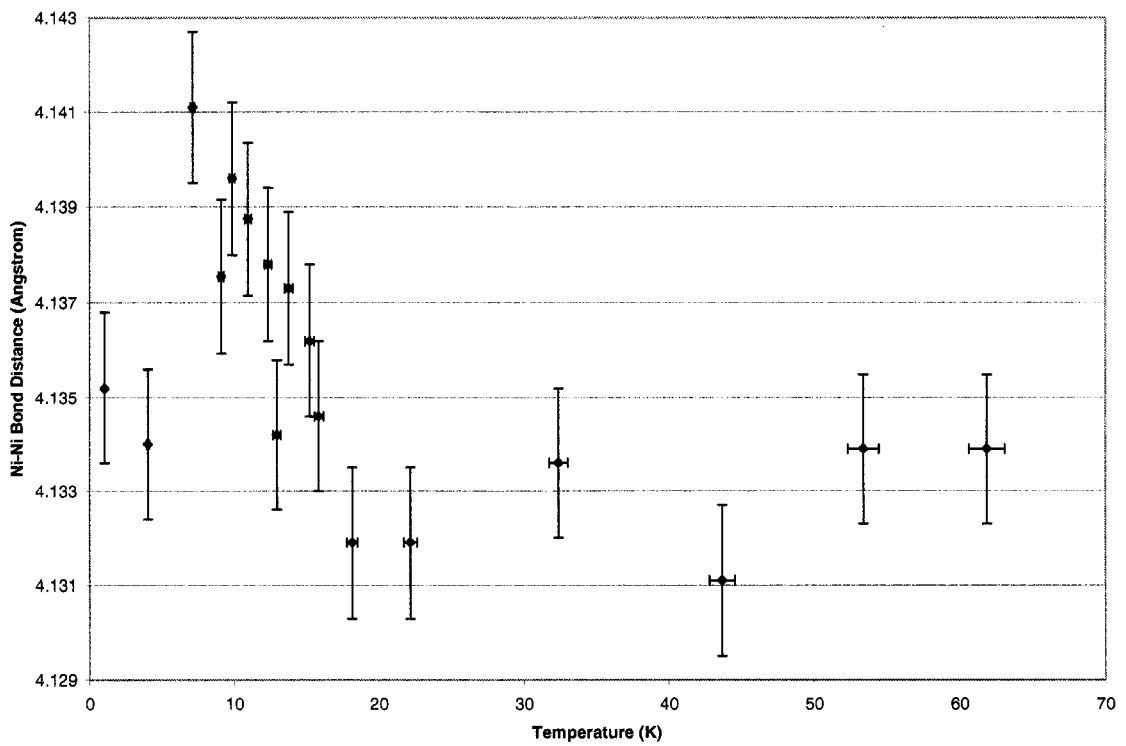
Figure 23. Ni-Ni bond distances versus temperature at Ni K Edge for $NiS_{1.38}Se_{0.62}$
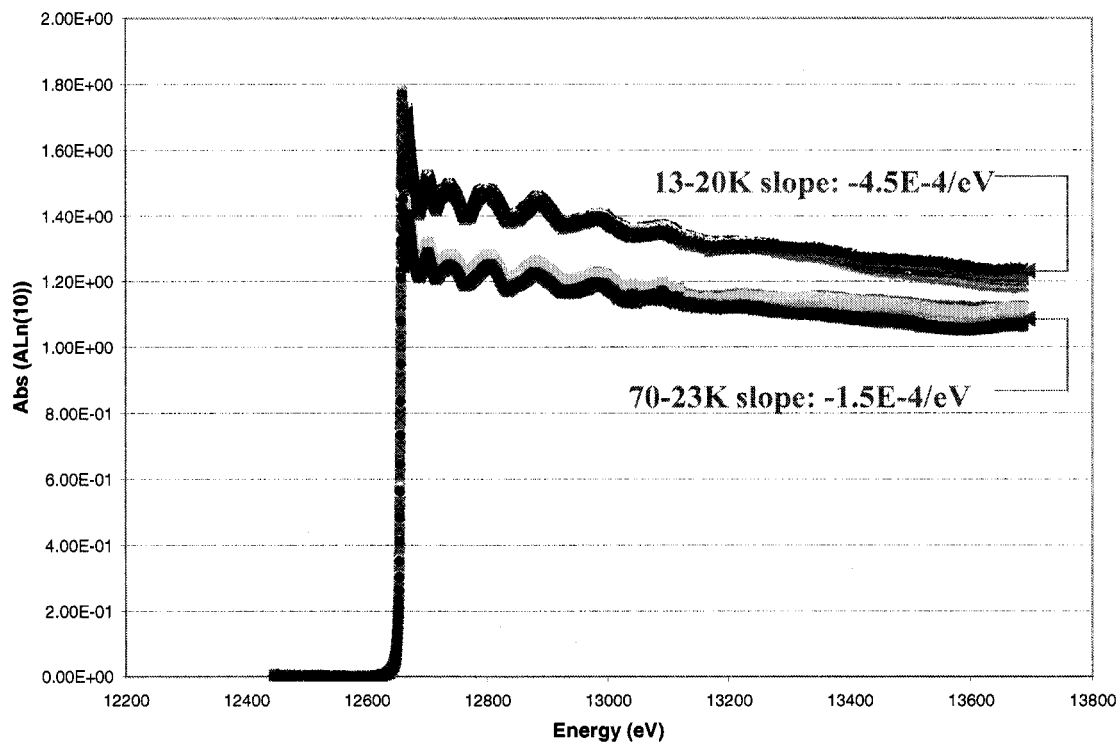
Figure 24. 2D plot of superimposed XAS spectrums from 2 K to 70 K of Se at K Edge of data file shown in Table 2 after data reduction using EXAFSPAK™
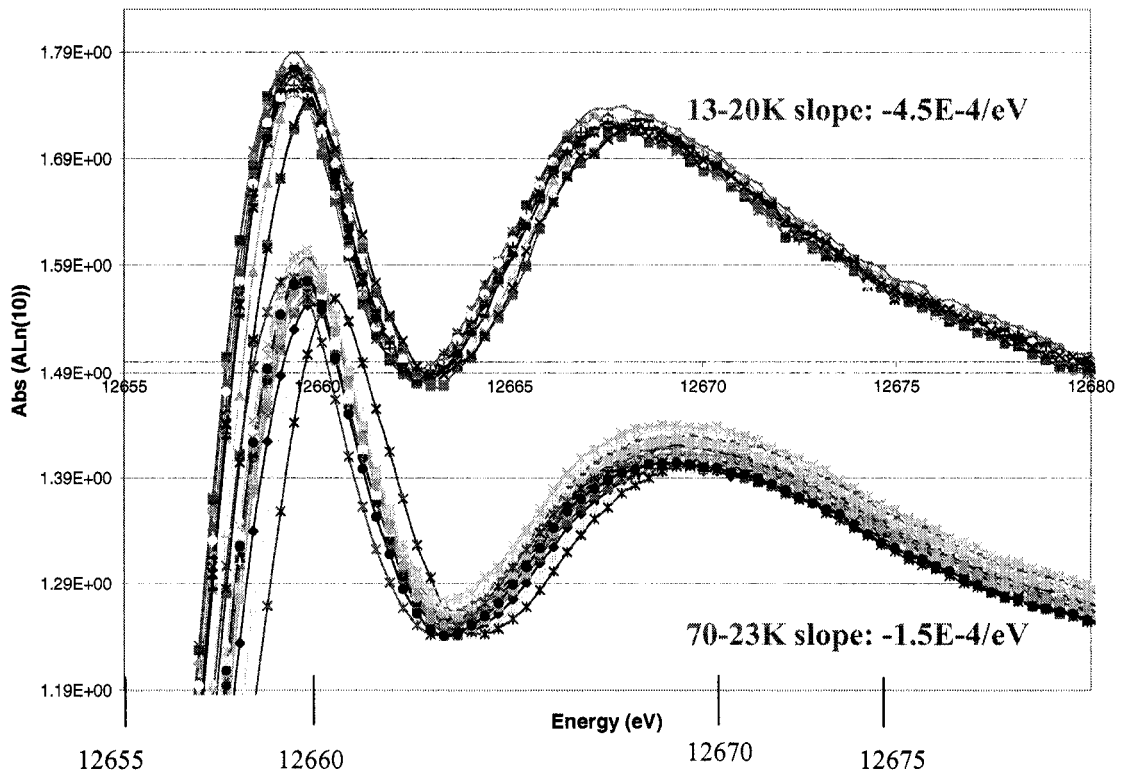
Figure 25. 2D plot of superimposed XAS spectrums magnified at EXAFS region of Se at K Edge of data file shown in Table 2 and Figure 24 after data reduction using EXAFSPAK™

Figure 26. 3D plot of superimposed XAS spectrums from 2 K to 70 K of Se at K Edge of data file shown in Table 2 after data reduction using EXAFSPAK™
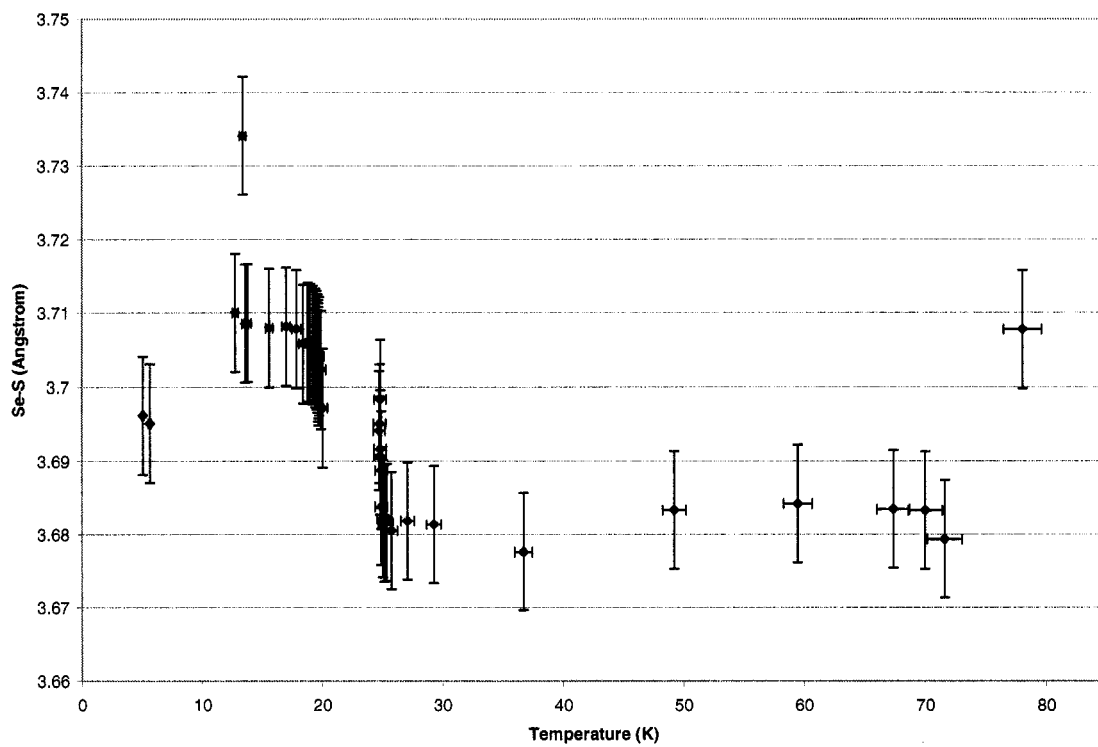
Figure 27. Se-S bond distances versus temperature at Se K Edge at Se K Edge for $NiS_{1.38}Se_{0.62}$

Se-Se Bond Distances vs Temperature at Se-K Edge

Figure 28. Se-Se bond distances versus temperature at Se K Edge at Se K Edge for $NiS_{1.38}Se_{0.62}$

Se-Ni Bond Distances vs. Temperature at Se-K Edge
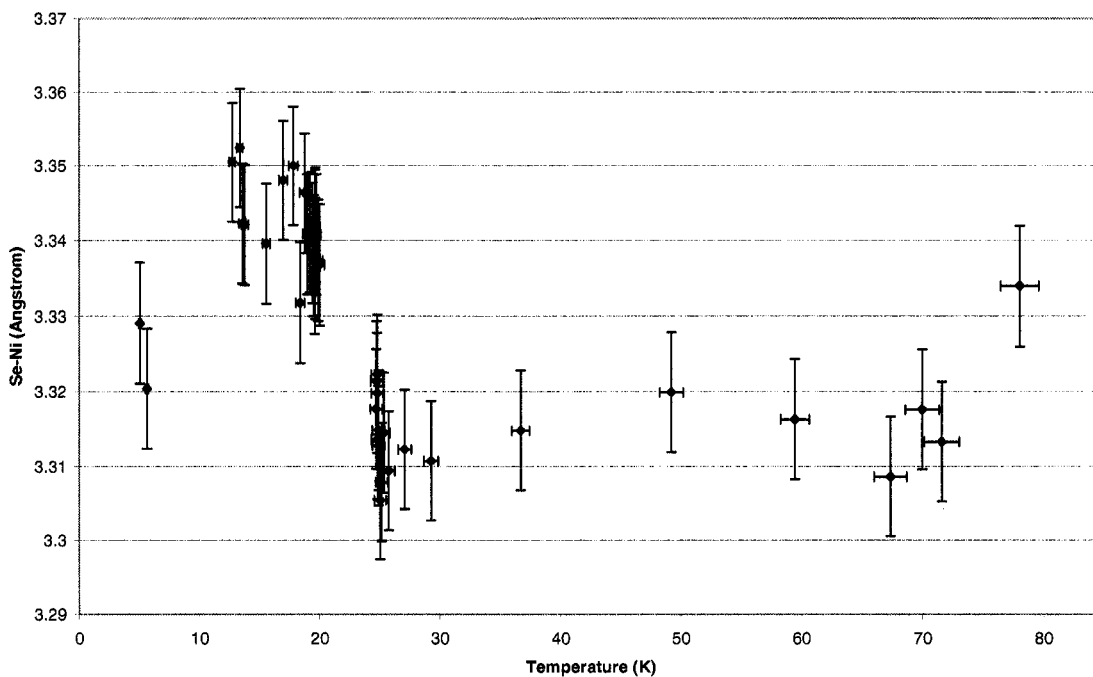
Figure 29. Se Ni bond distances versus temperature at Se K Edge at Se K Edge for $NiS_{1.38}Se_{0.62}$

XTDAS = A(T) − A(T$_{5K}$)

Perturbed State   **Normal State**   **Δ Due to Perturbation**
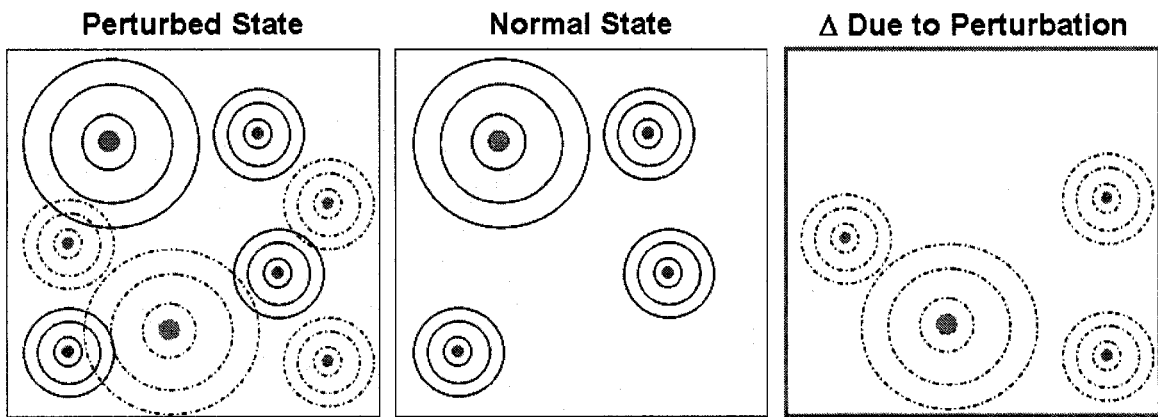
Figure 30. By subtracting XAS of a perturbed state from a normal state, the net result is changes in structural or electron density due to the effect of perturbation. Advantage of XTDAS in the study of phase transition is that only the bond responsible for the transition is selected

69
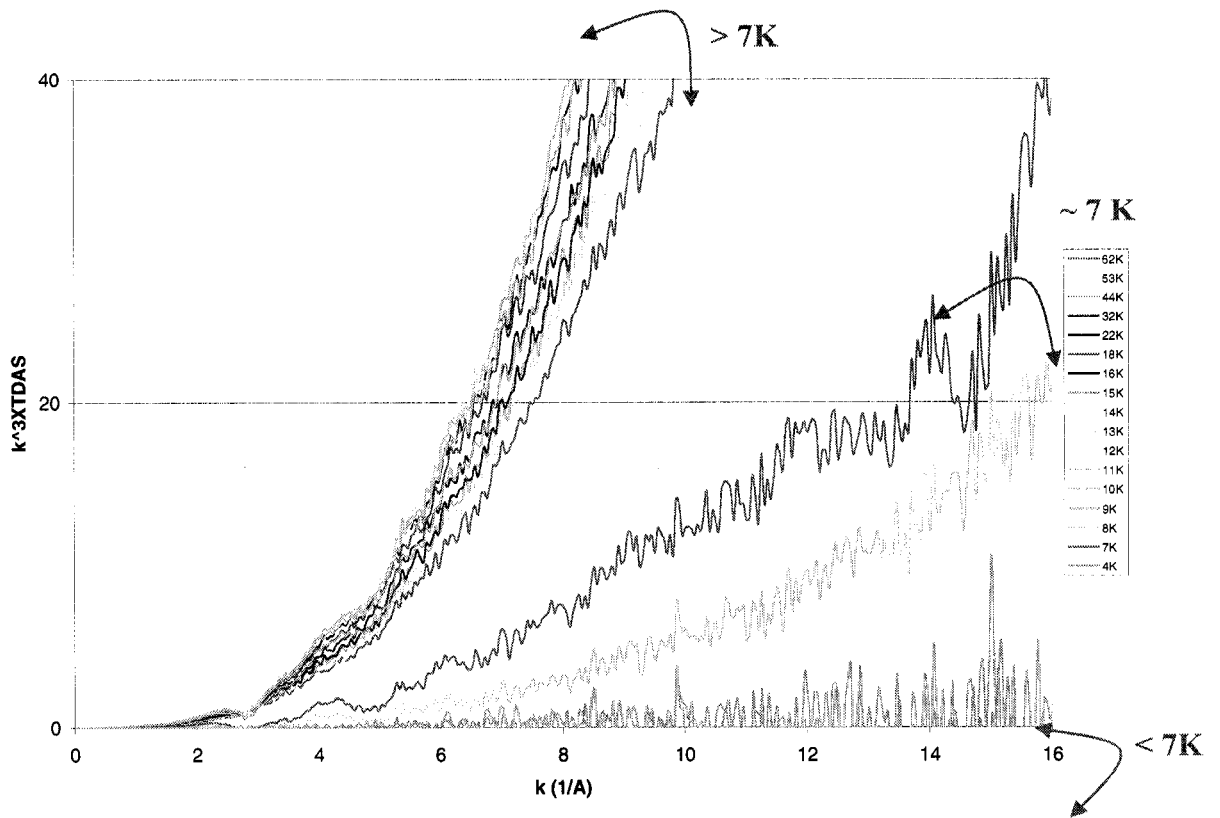
Figure 31. k^3XTDAS as function of k (1/A) at Ni K Edge for $NiS_{1.38}Se_{0.62}$. XTDAS data is obtained by taking Ni K Edge data for each temperature run from Table 1 and taking the difference of each data relative to the normal state at 5K. The result is multiply by k^3. Three temperature regions are identified – temperature less 7K, perturbation is negligible; at 7K relaxation time begins to change; higher than 7K, changes in relaxation time is more dramatic.
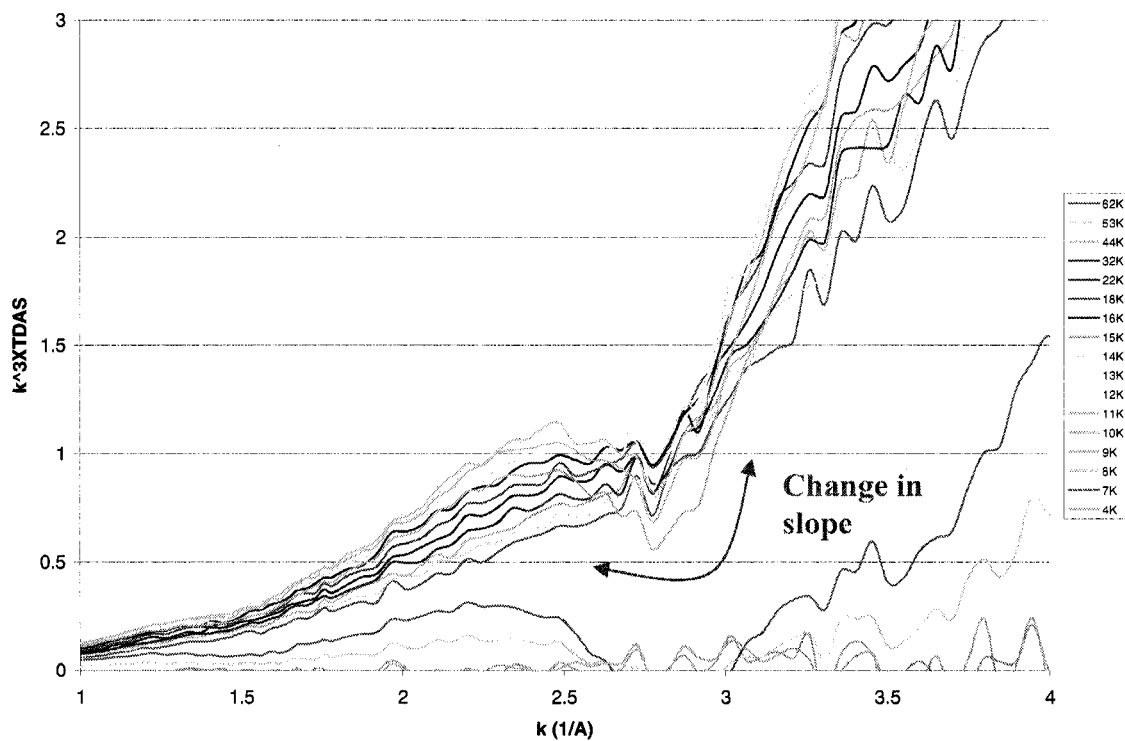
Figure 32. k^3XTDAS as function of k (1/A) at Ni K Edge magnified from
Figure 31

71

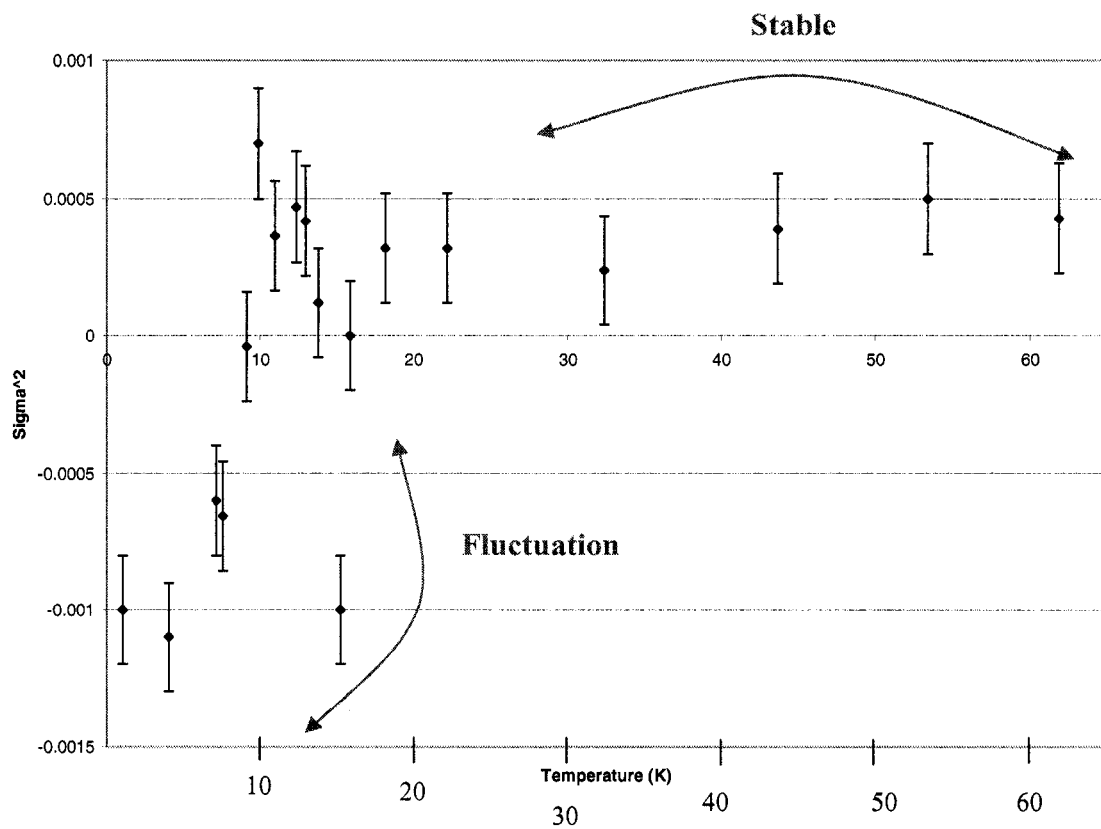Figure 33. Debye-Wall as function of temperature at Ni K Edge for $NiS_{1.38}Se_{0.62}$
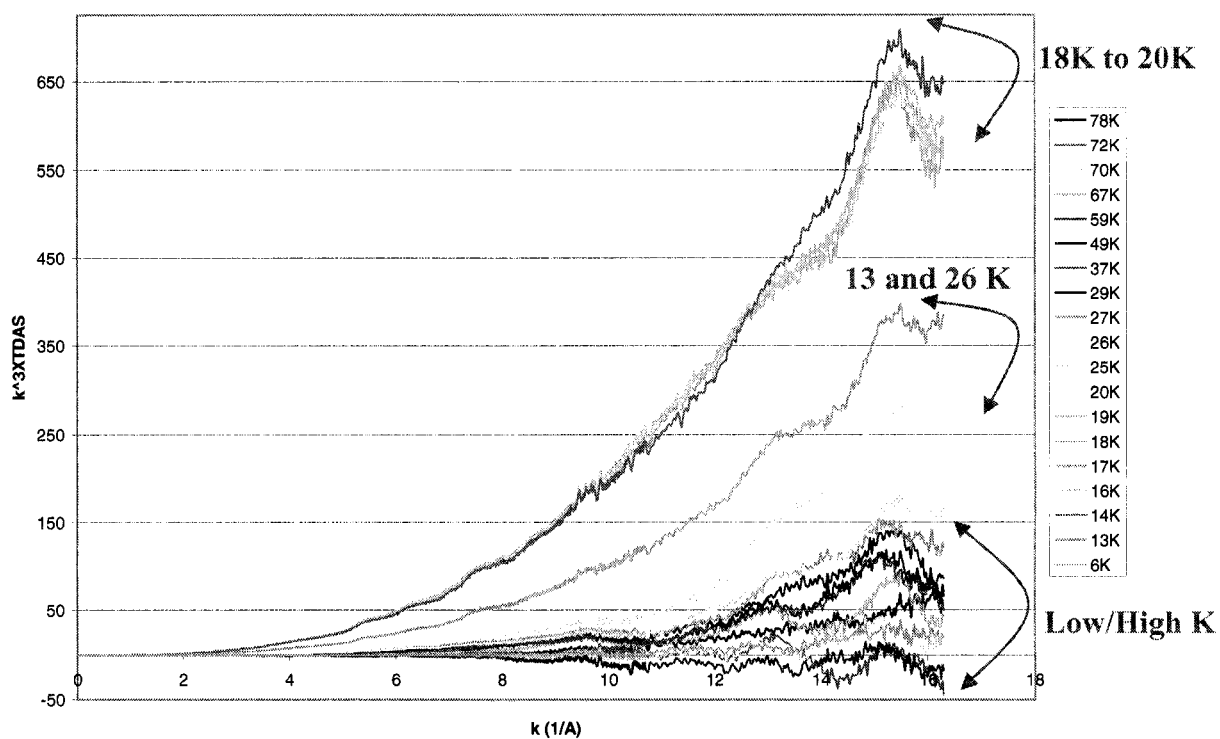
Figure 34. k^3XTDAS as function of k (1/A) at Se K Edge for $NiS_{1.38}Se_{0.62}$. XTDAS data is obtained by taking Se K Edge data for each temperature run from Table 2 and taking the difference of each data relative to the normal state at 5K. The result is multiply by k^3. Three temperature regions are identified – temperature from 18-20K, the changes in relaxation time is more dramatic; from 13-26K, relaxation time begins to change; temperature above 26K and below 13, perturbation is negligible
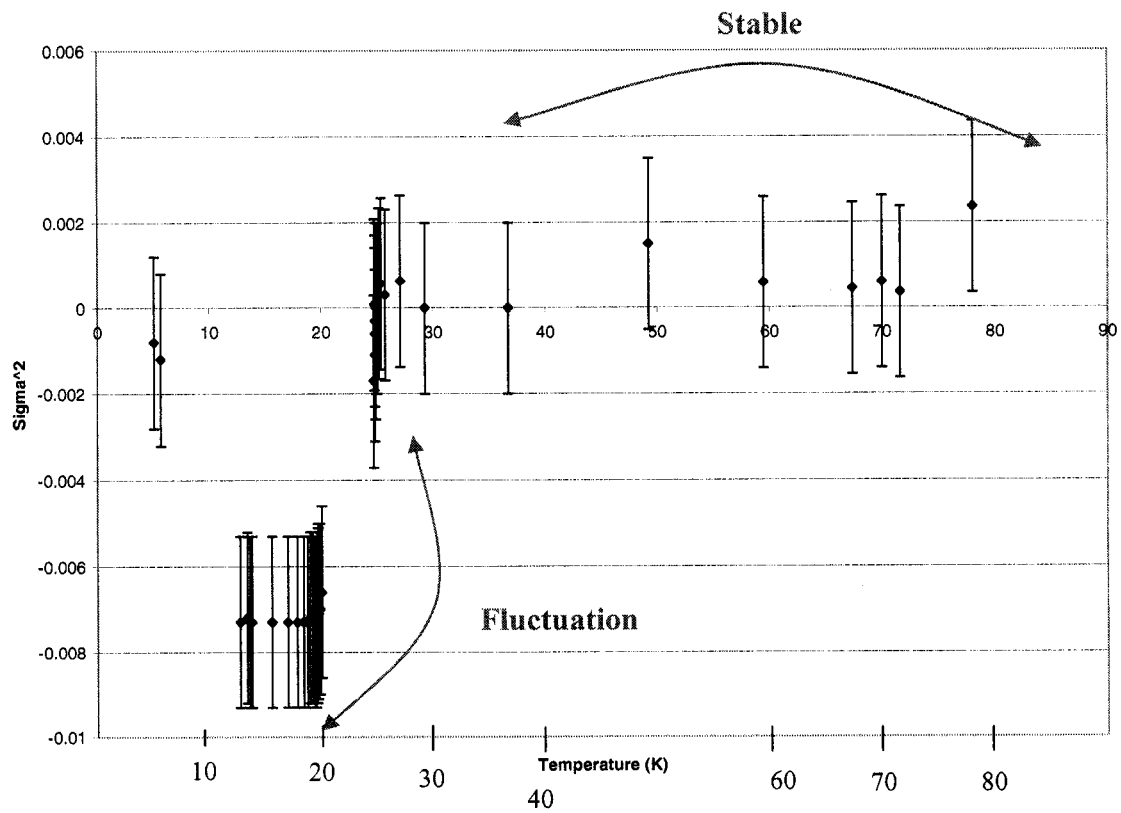
Figure 35. Debye-Wall as function of temperature at Se K Edge for $NiS_{1.38}Se_{0.62}$
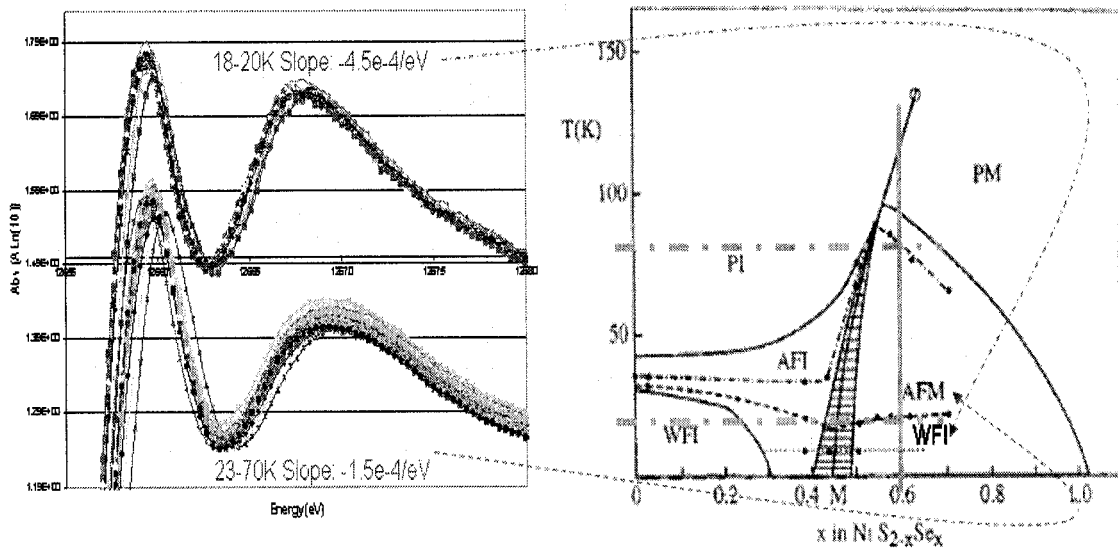
Figure 36. Correlation between XAS data at Se K Edge and phase diagram
suggests a phase transition from AF metal to WF insulator at 18 K